[31] R. Pankov, N. Neznanov, A. Umezawa, R.G. Oshima, AP-1, ETS, and transcriptional silencers regulate retinoic acid-dependent induction of keratin 18 in embryonic cells, Mol. Cell Biol. 14 (1994) 7744–7757.
[32] H. Nomura, H. Sato, M. Seiki, M. Mai, Y. Okada, Expression of membrane-type matrix metalloproteinase in human gastric carcinomas, Cancer Res. 55 (1995) 3263–3266.
[33] M. Tokuraku, H. Sato, S. Murakami, Y. Okada, Y. Watanabe, M. Seiki, Activation of the precursor of gelatinase A/72 kDa type IV collagenase/MMP-2 in lung carcinomas correlates with the expression of membrane-type matrix metalloproteinase (MT-MMP) and with lymph node metastasis, Int. J. Cancer 64 (1995) 355–359.
[34] H. Ueno, H. Nakamura, M. Inoue, K. Imai, M. Noguchi, H. Sato, M. Seiki, Y. Okada, Expression and tissue localization of membrane-types 1, 2, and 3 matrix metalloproteinases in human invasive breast carcinomas, Cancer Res. 57 (1997) 2055–2060.
[35] M. Nakada, H. Nakamura, E. Ikeda, N. Fujimoto, J. Yamashita, H. Sato, M. Seiki, Y. Okada, Expression and tissue localization of membrane-type 1, 2, and 3 matrix metalloproteinases in human astrocytic tumors, Am. J. Pathol. 154 (1999) 417–428.
[36] H. Nakamura, H. Ueno, K. Yamashita, T. Shimada, E. Yamamoto, M. Noguchi, N. Fujimoto, H. Sato, M. Seiki, Y. Okada, Enhanced production and activation of progelatinase A mediated by membrane-type 1 matrix metalloproteinase in human papillary thyroid carcinomas, Cancer Res. 59 (1999) 467–473.
[37] S.K. Chintala, R. Sawaya, Z.L. Gokaslan, J.S. Rao, Modulation of matrix metalloprotease-2 and invasion in human glioma cells by alpha 3 beta 1 integrin, Cancer Lett. 103 (1996) 201–208.
[38] Y. Kadono, Y. Okada, M. Namiki, M. Seiki, H. Sato, Transformation of epithelial Madin–Darby canine kidney cells with p60(v-src) induces expression of membrane-type 1 matrix metalloproteinase and invasiveness, Cancer Res. 58 (1998) 2240–2244.
[39] Y. Kadono, K. Shibahara, M. Namiki, Y. Watanabe, M. Seiki, H. Sato, Membrane type 1-matrix metalloproteinase is involved in the formation of hepatocyte growth factor/scatter factor-induced branching tubules in Madin–Darby canine kidney epithelial cells, Biochem. Biophys. Res. Commun. 251 (1998) 681–687.
[40] L. Long, R. Navab, P. Brodt, Regulation of the Mr 72,000 type IV collagenase by the type I insulin-like growth factor receptor, Cancer Res. 58 (1998) 3243–3247.
[41] A. Llorens, I. Rodrigo, L. Lopez-Barcons, M. Gonzalez-Garrigues, E. Lozano, A. Vinyals, M. Quintanilla, A. Cano, A. Fabra, Down-regulation of E-cadherin in mouse skin carcinoma cells enhances a migratory and invasive phenotype linked to matrix metalloproteinase-9 gelatinase expression, Lab. Invest. 78 (1998) 1131–1142.
[42] S. Kubota, H. Ito, Y. Ishibashi, Y. Seyama, Anti-alpha3 integrin antibody induces the activated form of matrix metalloprotease-2 (MMP-2) with concomitant stimulation of invasion through matrigel by human rhabdomyosarcoma cells, Int. J. Cancer 70 (1997) 106–111.
[43] W.A. May, A. Arvand, A.D. Thompson, B.S. Braun, M. Wright, C.T. Denny, EWS/FLI1-induced manic fringe renders NIH 3T3 cells tumorigenic, Nat. Genet. 17 (1997) 495–497.
[44] A.D. Thompson, B.S. Braun, A. Arvand, S.D. Stewart, W.A. May, E. Chen, J. Korenberg, C. Denny, EAT-2 is a novel SH2 domain containing protein that is up regulated by Ewing sarcoma EWS/FLI1 fusion gene, Oncogene 13 (1996) 2649–2658.
[45] A. Umezawa, H. Yamamoto, L. Rhodes, M. Klemsz, R. Maki, R. Ohshima, Methylation of an ETS site in the intron enhancer of the keratin 18 gene participates in tissue-specific repression, Mol. Cell. Biol. 17 (1997) 4885–4894.

THE JOURNAL OF BIOLOGICAL CHEMISTRY
Vol. 277, No. 46, Issue of November 15, pp. 43730–43734, 2002
Printed in U.S.A.

Phosphorylation and Inactivation of Myeloid Cell Leukemia 1 by JNK in Response to Oxidative Stress*

Received for publication, August 5, 2002, and in revised form, September 4, 2002
Published, JBC Papers in Press, September 9, 2002, DOI 10.1074/jbc.M207951200

Seiji Inoshita‡§, Kohsuke Takeda‡, Takiko Hatai‡, Yoshio Terada§, Makoto Sano¶, Junichi Hata¶, Akihiro Umezawa¶, and Hidenori Ichijo‡‖

From the ‡Laboratory of Cell Signaling, Department of Hard Tissue Engineering, Division of Bio-Matrix, §Homeostasis Medicine and Nephrology, Department of Regulation of Internal Environment and Reproduction, Division of Systemic Organ Regulation, Graduate School, Tokyo Medical and Dental University, 1-5-45 Yushima, Bunkyo-ku, Tokyo 113-8549, Japan, and the ¶Department of Pathology, Keio University School of Medicine, 35 Shinanomachi, Shinjuku-ku, Tokyo 160-8582, Japan

Oxidative stress induces JNK activation, which leads to apoptosis through mitochondria-dependent caspase activation. However, little is known about the mechanism by which JNK alters mitochondrial function. In this study, we investigated the role of phosphorylation of myeloid cell leukemia 1 (Mcl-1), an anti-apoptotic member of the Bcl-2 family, in oxidative stress-induced apoptosis. We found that JNK phosphorylated Ser-121 and Thr-163 of Mcl-1 in response to stimulation with H_2O_2 and that transfection of unphosphorylatable Mcl-1 resulted in an enhanced anti-apoptotic activity in response to stimulation with H_2O_2. JNK-dependent phosphorylation and thus inactivation of Mcl-1 may be one of the mechanisms through which oxidative stress induces cellular damage.

Oxidative stress has been implicated in the pathogenesis of several abnormal conditions and diseases including ischemia, cancer, and diabetes mellitus (1–3). A recent study suggests that stress-activated protein kinases such as JNK[1] and p38 play important roles in triggering apoptosis in response to various cellular stressors including oxidative stress. We have shown that oxidative stress-induced sustained activation of JNK and p38 is required for apoptosis (4). Apoptosis signal-regulating kinase 1 (ASK1), a member of the mitogen-activated protein kinase (MAPK) kinase kinase (MAPKKK), specifically mediates the sustained activation of JNK/p38 and apoptosis in response to oxidative stress (5, 6). ASK1-dependent apoptosis is mediated by the release of cytochrome *c* from the mitochondria followed by caspase 9 activation (7). It has also been reported that JNK is required for UV-induced release of cytochrome *c* and that new gene expression is not required for this process (8). These reports indicate that JNK induces apoptosis in part through the mitochondria-dependent caspase activation. However, the molecular mechanism by which activated JNK induces mitochondrial dysfunction is unclear.

The members of the Bcl-2 family play pivotal roles in cellular decision to undergo apoptosis. Bcl-2 has been reported to be phosphorylated by JNK in response to different stimuli (9–11). Although the significance of phosphorylation of Bcl-2 is controversial, it was suggested that phosphorylation by JNK within the unstructured loop region of Bcl-2 decreases its anti-apoptotic activity (9, 10, 12). Anti-apoptotic Bcl-2 family proteins thus may be potential mediators of JNK-induced apoptosis. However, little is known about the relation between JNK and the other anti-apoptotic members of the Bcl-2 family in the context of oxidative stress-induced apoptosis signaling.

The myeloid cell leukemia 1 (Mcl-1) (13), also known as EAT (14), is an anti-apoptotic Bcl-2 family member. Mcl-1 plays an important role in the development of various carcinomas (15–17). Similar to other Bcl-2 family members, Mcl-1 localizes in the mitochondrion as well as in other intracellular membranes (18) and can associate with other pro-apoptotic family members (19). Mcl-1 differs from Bcl-2 and Bcl-XL in structure (13), in its short half-life (13), in the regulation of its promoter (20–22), and in its ability to protect cells from a variety of cytotoxic stimuli (23, 24). Little is known regarding posttranslational modification and regulation of Mcl-1. In this study, we investigated the potential involvement of phosphorylation regulation of Mcl-1.

EXPERIMENTAL PROCEDURES

Cell Culture and Transfection—HEK293 cells were grown under 5% CO_2 in Dulbecco's modified Eagle's medium containing 10% fetal bovine serum, 4.5 g/liter glucose, and 100 units/ml penicillin. Porcine aortic endothelial (PAE) cells were grown under 5% CO_2 in F12 medium (Invitrogen) supplemented with 10% fetal bovine serum, 10 mM HEPES, and 100 units/ml penicillin. Transfection with various constructs in pGEX-Neo was performed using 2 μg of plasmid and 8 μl of Tfx 50 (Promega). Transfected cells were selected in the presence of 1 mg/ml Geneticin for 2 weeks, and drug-resistant single-cell colonies were chosen and maintained in growth medium containing 0.4 mg/ml Geneticin.

Antibodies and Reagents—Rabbit polyclonal antibody to Mcl-1 was purchased from BD Biosciences. Phospho-JNK (Thr-183/Tyr-185) and p38 (Thr-180/Tyr-182) were purchased from New England Biolabs. Phospho-ERK (Thr-183/Tyr-185) was purchased from Promega. The antibodies to Myc tag (clone 9E10), HA tag (clone 3F10), and FLAG tag were purchased from Calbiochem, Roche Molecular Biochemicals, and Sigma, respectively. SB203580 was purchased from Calbiochem.

Western Blot Analysis—Cells were lysed in a lysis buffer containing 150 mM NaCl, 50 mM Tris-HCl, pH 8.0, 1% Nonidet P-40, 0.5% deoxycholate, 0.1% SDS, 1 mM DTT, 1 mM phenylmethylsulfonyl fluoride, and

* This work was supported by grants-in-aid for scientific research from the Ministry of Education, Culture, Sports, Science, and Technology of Japan. The costs of publication of this article were defrayed in part by the payment of page charges. This article must therefore be hereby marked "*advertisement*" in accordance with 18 U.S.C. Section 1734 solely to indicate this fact.

‖ Present address and to whom correspondence should be addressed: Laboratory of Cell Signaling, Graduate School of Pharmaceutical Sciences, University of Tokyo, 7-3-1 Hongo, Bunkyo-ku, Tokyo 113-0033, Japan. Tel.: 81-3-5841-4859; Fax: 81-3-5841-4778; E-mail: ichijo@mol.f.u-tokyo.ac.jp.

[1] The abbreviations used are: JNK, c-Jun NH_2-terminal kinase; ASK, apoptosis signal-regulating kinase; MAPK, mitogen-activated protein kinase; MAPKKK, MAPK kinase kinase; Mcl-1, myeloid cell leukemia 1; PAE, porcine aortic endothelial; ERK, extracellular signal-regulated kinase; HA, hemagglutinin; DTT, dithiothreitol; GST, glutathione *S*-transferase; WT, wild type.

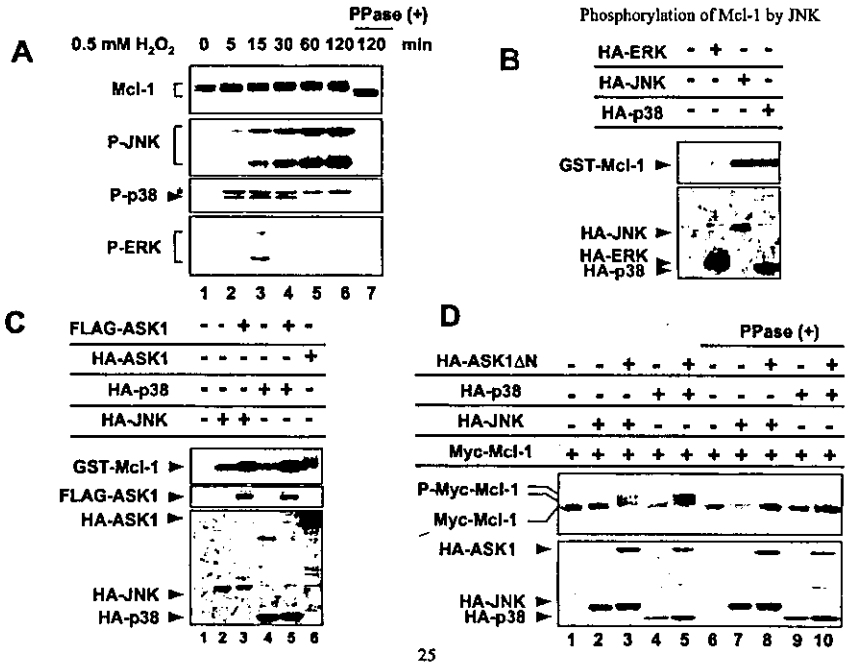

25

FIG. 1. **Phosphorylation of Mcl-1 by JNK and p38.** *A*, H_2O_2-induced Mcl-1 phosphorylation. PAE cells were treated with 0.5 mM H_2O_2 for the indicated periods of time. Cells were lysed in a lysis buffer for the phosphatase treatment. Aliquots of the samples were incubated with (*PPase*(+)) or without λ protein phosphatase at 30 °C for 30 min. Western blots were performed using the indicated specific antibodies. *Asterisk* indicates nonspecific band. *B*, phosphorylation of Mcl-1 by JNK and p38 *in vitro*. HEK 293 cells were transfected as indicated. 24 h after transfection, HA-MAPKs were immunoprecipitated with an anti-HA monoclonal antibody. *In vitro* kinase assay was performed using GST-Mcl-1 as the substrate. *Upper panel*, phosphorylation of GST-Mcl-1; *lower panel*, Western blotting of HA-MAPK kinases in the lysate. *C*, kinase activation-dependent phosphorylation of Mcl-1 *in vitro*. HEK293 cells were transfected as indicated. 24 h after transfection, HA-tagged proteins were immunoprecipitated with an anti-HA monoclonal antibody. *In vitro* kinase assay was performed as described above. *Top*, phosphorylation of GST-Mcl-1; *middle*, Western blotting of FLAG-ASK1 in the lysate; *bottom*, Western blotting of HA-MAPKs. *D*, phosphorylation of Mcl-1 by activated JNK and p38 *in vivo*. Myc-Mcl-1 was transfected into 293 cells in combination with HA-ASK1ΔN, which is a constitutively active mutant of ASK1, HA-JNK, and HA-p38 as indicated. 24 h after transfection, cells were lysed in a lysis buffer for phosphatase treatment and incubated with or without λ-protein phosphatase. Samples were immunoblotted using anti-Myc antibody (*upper panel*) and anti-HA antibody (*lower panel*).

1.5% aprotinin. Cell extracts were clarified by centrifugation and resolved on SDS-PAGE followed by electroblotting onto polyvinylidene difluoride membrane. After blocking with 5% skim milk in Tris-buffered saline with Tween 20 (150 mM NaCl, 50 mM Tris-HCl, pH 8.0, and 0.05% Tween 20), the membranes were probed with antibodies. The antibody-antigen complexes were detected using the ECL system (Amersham Biosciences).

Construction of Expression Plasmids and an Adenovirus Vector—A cDNA clone containing the full-length of the Mcl-1 coding region was inserted into pcDNA3.0 vector. To replace Ser-121 and/or Thr-163 with Ala, a PCR-based site-directed mutagenesis method was used. The Myc tag was inserted at the NH_2 termini of wild type and mutant Mcl-1. pcDNA3-HA-ERK, pcDNA3-HA-JNK, pcDNA3-HA-p38, pcDNA3-HA-ASK1, pcDNA3-HA-ASK1ΔN, and pcDNA3-FLAG-ASK1 have been described previously (6, 26–28).

Recombinant adenovirus was constructed as described elsewhere (29, 30). MKK4 cDNA was subcloned in pcDNA3 by PCR. Lys-116 was replaced by Arg using a PCR-based site-directed mutagenesis method. Green fluorescent protein-tagged MKK4 mutant cDNA was subcloned into the *Swa*I site of pAdex1pCAw cassette cosmid. Each cosmid bearing the expression unit and adenovirus DNA-terminal protein complex was cotransfected into the E1 transcomplementing 293 cell clone. The recombinant adenoviruses generated by homologous recombination were isolated, and high titer stocks of recombinant adenoviruses were grown in 293 cells and purified. Nearly 100% infection of PAE cells by recombinant adenoviruses can be achieved at a m.o.i. of 100 as determined by green fluorescent protein fluorescence (data not shown).

In Vitro Kinase Assay—A cDNA encoding the human Mcl-1 protein corresponding to amino acids 31–229 was inserted into the pGEX-2T expression vector (Amersham Biosciences). Mcl-1-GST protein was induced in *Escherichia coli* BL21 cells by adding 0.5 mM isopropyl-β-D-thiogalactopyranoside and purified with glutathione-Sepharose 4B (Amersham Biosciences). The immune complex kinase assay was done as described previously (26). The indicated plasmids were co-transfected into 293 cells by Tfx 50 (Promega). Cells were lysed in a lysis buffer containing 150 mM NaCl, 20 mM Tris-HCl, pH 7.5, 5 mM EGTA, 1% Triton X-100, 1% deoxycholate, 12 mM β-glycerophosphate, 50 mM NaF, 1 mM sodium orthovanadate, 1 mM DTT, 1 mM phenylmethylsulfonyl fluoride, and 1.5% aprotinin. Cell extracts were clarified by centrifugation, and the supernatants were immunoprecipitated with anti-HA antibody using protein A-Sepharose (Zymed Laboratories Inc.). The beads were washed twice with washing buffer (150 mM NaCl, 20 mM Tris-HCl, pH 7.5, 5 mM EGTA, and 1 mM DTT), and then incubated with GST-Mcl-1 as the substrate for 20 min at 30 °C in 30 μl of kinase buffer (20 mM Tris-HCl, pH 8.0, 20 mM $MgCl_2$, and 0.3 μCi of [γ-^{32}P]ATP). The kinase reaction was stopped by adding SDS sample buffer and analyzed by SDS-PAGE and a Fuji BAS2000 Image analyzer.

Phosphatase Treatment—Cells were lysed in a lysis buffer for phosphatase treatment containing 150 mM NaCl, 10 mM Tris-HCl, pH 7.5, 1 mM EDTA, 1% Nonidet P-40, 1 mM DTT, 1 mM phenylmethylsulfonyl fluoride, and 1.5% aprotinin. Cellular debris was removed by centrifugation. Lysates were incubated with or without 2 units/μl of λ-protein phosphatase (New England Biolabs) according to the instructions provided by the manufacturer. The reaction was terminated by adding SDS sample buffer and boiling for 3 min.

Metabolic Labeling—Cells were incubated in phosphate-free medium containing 0.1% fetal bovine serum and 10 mM HEPES, pH 7.0, at 37 °C for 3 h. [^{32}P]Orthophosphate (Amersham Biosciences) was then added at a final concentration of 1 mCi/ml, and labeling was continued at 37 °C for 3 h. The cells were transferred onto ice and washed twice with ice-cold phosphate-buffered saline and then lysed and immunoprecipitated with anti-Myc antibody and analyzed by SDS-PAGE.

Analysis of Cell Viability—Cells were stimulated with 0.5 mM H_2O_2 containing F12 medium for 3 h. Cell viability was measured by the trypan blue (Sigma) dye exclusion method. Cells were trypsinized, centrifuged, resuspended in phosphate-buffered saline, and counted using a hemocytometer after dilution in trypan blue. Blue cells were considered as dead cells.

RESULTS

To investigate whether Mcl-1 is regulated by phosphorylation in response to oxidative stress, PAE cells were exposed to

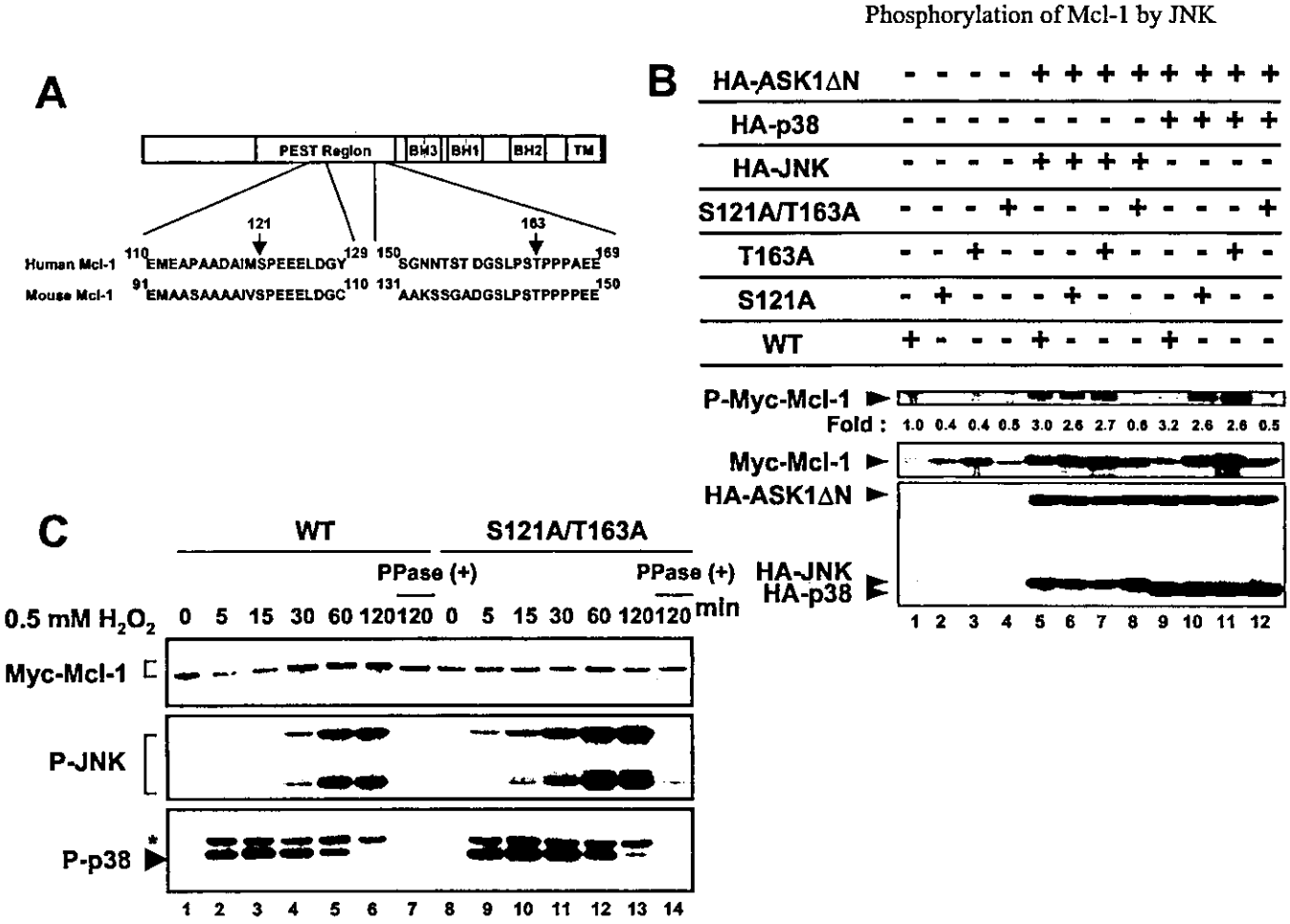

FIG. 2. **Mcl-1 is phosphorylated on serine 121 and threonine 163.** *A*, schematic representation of Mcl-1 and the conserved MAPK phosphorylation sites. The sequence of human and mouse Mcl-1 containing the conserved MAPK phosphorylation sites are shown. We constructed NH_2-terminally Myc-tagged plasmids encoding wild type (*WT*), a single alanine substitution mutant (S121A and T163A) and a double alanine substitution mutant (S121A/T163A) of Mcl-1. *B*, phosphorylation sites of Mcl-1 by JNK and p38. 293 cells were transfected with WT or mutants S121A, T163A, and S121A/T163A of Mcl-1 in combination with ASK1ΔN-HA, JNK-HA, and p38-HA as indicated. Cells were incubated in the medium without phosphate for 3 h and labeled with [^{32}P]orthophosphate for another 3 h. Mcl-1 was then immunoprecipitated with an anti-Myc antibody and separated by 8.5% PAGE. *Top*, phosphorylated Mcl-1 was detected by an image analyzer; *middle*, Western blotting of Myc- Mcl-1 in the lysate; *bottom*, Western blotting of HA-MAPKs and HA-ASK1 in the lysate. The intensity of Mcl-1 phosphorylation relative to amount of Mcl-1 protein was calculated, and the intensity was shown as fold increase relative to control. *C*, the absence of gel mobility shift of S121A/T163A Mcl-1 on H_2O_2 treatment. PAE clones stably expressing WT or S121A/T163A MCL-1 were treated with 0.5 mM H_2O_2 for the indicated periods of time. Cells were lysed in a lysis buffer for phosphatase treatment. Aliquots of the samples were incubated with or without λ-protein phosphatase at 30 °C for 30 min. Western blots were performed using the indicated specific antibodies. *Asterisk* indicates nonspecific band.

H_2O_2 and the electrophoretic mobility of Mcl-1 was assessed by immunoblotting analysis. We detected endogenous Mcl-1 of PAE cells as a double band under non-stressed conditions (Fig. 1*A*, *top*, *lane* 1). The mobility of both bands was delayed by H_2O_2 treatment in a time-dependent manner (Fig. 1*A*, *top*, *lanes 2–6*). The treatment of cell lysates prepared from H_2O_2-stimulated (Fig. 1*A*, *top*, *lane 7*) and unstimulated (data not shown) PAE cells with λ-protein phosphatase resulted in the acceleration of the mobility of those bands. These findings suggest that endogenous Mcl-1 is partially phosphorylated under non-stressed conditions and that additional phosphorylation occurred after H_2O_2 treatment.

To identify the kinase responsible for Mcl-1 phosphorylation in response to H_2O_2, we examined the activation state of three classes of MAPK, namely, ERK, JNK, and p38, which are all known to be activated by H_2O_2 (4, 31). The kinetics of activation of JNK correlated with the extent of mobility of Mcl-1 (Fig. 1*A*), suggesting that JNK might be involved in the H_2O_2-induced phosphorylation of Mcl-1. To examine which MAPK can phosphorylate Mcl-1 directly, we carried out an *in vitro* kinase assay using recombinant Mcl-1 as the substrate. JNK and p38 strongly phosphorylated Mcl-1 *in vitro*, whereas the phosphorylation of Mcl-1 by ERK was marginal (Fig. 1*B*). The co-transfection of ASK1, a MAPKKK that activates JNK and that p38 MAPK cascades *in vivo*, strongly enhanced the phosphorylation of Mcl-1 by JNK and p38 (Fig. 1*C*, *top*, *lanes 1–5*). ASK1 itself phosphorylated Mcl-1 very weakly (Fig. 1*C*, *top*, *lane 6*). These findings suggested that Mcl-1 may serve as a specific substrate for JNK and p38 at least *in vitro*. We next examined whether Mcl-1 could be phosphorylated by JNK and p38 in mammalian cells. When Mcl-1 was co-transfected with JNK or p38 alone, the phosphorylation of Mcl-1 was undetectable as determined by the band shift analysis (Fig. 1*D*, *lanes 2* and *4*). In contrast, Mcl-1 became a shifted doublet by the co-expression of the activated allele of ASK1 (ASK1ΔN) together with JNK or p38 (Fig. 1*D*, *lanes 3* and *5*). Phosphatase

treatment shifted the doublet down to the basal status (Fig. 1*D*, *lanes 6–10*), indicating that activated JNK and p38 could phosphorylate Mcl-1 *in vivo*.

A sequence comparison of human and mouse Mcl-1 revealed that Mcl-1 possesses two conserved sites, Ser-121 and Thr-163, in humans that conforms to the consensus motif for the substrate of JNK and p38 (Fig. 2*A*). These sites are located in the PEST (proline, glutamic acid, serine, and threonine) domain of Mcl-1 (Fig. 2*A*) and correspond to the so-called unstructural loop region in Bcl-2, which regulates the anti-apoptotic function of Bcl-2 (32). To examine which sites are phosphorylated by JNK or p38, we constructed three alanine substitution mutants of Mcl-1 (S121A, T163A, and S121A/T163A). The Myc-tagged wild-type (WT) or alanine-substituted mutant of Mcl-1 was co-transfected with JNK or p38 plus ASK1ΔN. Cells were metabolically labeled with [^{32}P]orthophosphate and analyzed by autoradiography after immunoprecipitation using anti-Myc antibody. WT and single alanine substitution mutants (S121A and T163A) of Mcl-1 were clearly phosphorylated by the co-expression of activated JNK and p38 (Fig. 2*B*, *top*, *lanes 5–7* and *9–11*). In contrast, little phosphorylation was detected in the double-alanine mutant (S121A/T163A) of Mcl-1 (Fig. 2*B*, *top*, *lanes 8* and *12*). These findings suggested that when overexpressed, activated JNK and p38 can phosphorylate both Ser-121 and Thr-163 of Mcl-1 and that these two amino acids are the major phosphorylation sites of Mcl-1 *in vivo*.

To investigate the involvement of Ser-121 and Thr-163 in oxidative stress-induced phosphorylation of Mcl-1 as observed in Fig. 1*A*, we generated PAE cell clones stably expressing Myc-tagged WT and S121A/T163A mutant of Mcl-1. When these cells were treated with H_2O_2, the activations of endogenous JNK and p38 were clearly observed in both cells in a time-dependent manner (Fig. 2*C*, *middle* and *bottom panels*). In parallel with JNK activation, gel mobility of Mcl-1 was retarded in WT but not in S121A/T163A mutant-expressing cells (Fig. 2*C*, *top*), and the retardation was canceled by treatment with λ-protein phosphatase (Fig. 2*C*, *lane 7*). We have examined three independently selected clones of WT and mutant Mcl-1 and obtained essentially the same results in independent clones (data not shown). These results suggest that both Ser-121 and Thr-163 of Mcl-1 are phosphorylated in response to oxidative stress.

The overexpression of either activated JNK or p38 phosphorylated Mcl-1 *in vivo* (Figs. 1*D* and 2*B*), and both kinases were activated by H_2O_2 treatment (Figs. 1*A* and 2*C*). However, time course analysis indicated that the activation of JNK coincided with Mcl-1 phosphorylation following H_2O_2 stimulation much better than that of p38 (Figs. 1*A* and 2*C*). To examine which signaling pathway is physiologically required for Mcl-1 phosphorylation in response to H_2O_2, we used the p38 inhibitor SB203580 and a recombinant adenovirus encoding dominant negative MKK4. Although p38 was specifically inactivated by SB203580 (data not shown), the treatment of PAE cells with SB203580 before H_2O_2 stimulation did not alter H_2O_2-induced Mcl-1 mobility shift (Fig. 3*A*). In contrast, the expression of the dominant negative MKK4 significantly reduced the gel mobility shift of Mcl-1 upon H_2O_2 treatment (Fig. 3*B*). JNK but not p38 activation was specifically reduced by adenovirus encoding dominant negative MKK4. Taken together, Mcl-1 appears to be phosphorylated mainly via the JNK pathway in response to oxidative stress.

Finally, we assessed the functional importance of Mcl-1 phosphorylation in oxidative stress-induced apoptosis. To this end, the susceptibility to H_2O_2-induced apoptosis was examined in PAE clones stably expressing WT and those expressing S121A/T163A Mcl-1. PAE clones were treated with 0.5 mM

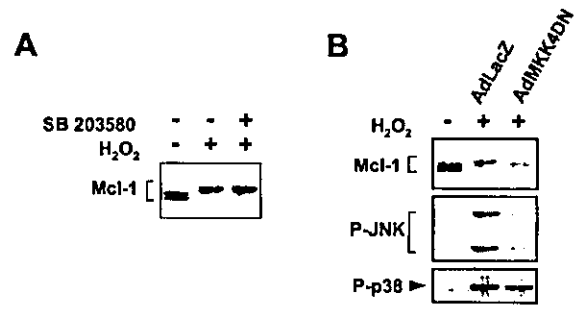

FIG. 3. **Requirement of the JNK pathway for H_2O_2-induced Mcl-1 phosphorylation.** *A*, involvement of p38 pathway in H2O2-induced Mcl-1 phosphorylation. PAE cells were treated with 10 μM SB203580 for 30 min followed by stimulation with 0.5 mM H_2O_2 for 60 min. Cells were lysed and immunoblotted using anti-Mcl-1 antibody. *B*, inhibition of H_2O_2-induced Mcl-1 phosphorylation by dominant negative MKK4. PAE cells were infected with 400 m.o.i. of a recombinant adenovirus encoding green fluorescent protein-tagged dominant negative MKK4 (*AdMKK4DN*). 24 h after the infection, the cells were treated with 0.5 mM H_2O_2 for 60 min. Cells were lysed and immunoblotted with an anti-Mcl-1 antibody.

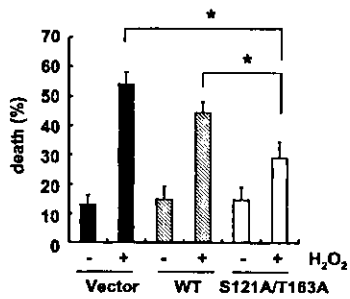

FIG. 4. **Enhancement of anti-apoptotic activity of Mcl-1 by substitution of phosphorylation sites for alanine.** PAE clones stably expressing WT or S121A/T163A MCL-1 were treated with 0.5 mM H_2O_2 for 3 h. Cell death was detected by trypan blue exclusion assay. Results are the mean ± S.E. of three independent experiments (*, $p < 0.05$).

H_2O_2 for 3 h, and cell death was determined by the trypan blue exclusion assay (Fig. 4). WT Mcl-1 conferred only minimal resistance compared with the vector control. However, S121A/T163A Mcl-1 showed substantially stronger anti-apoptotic activity than WT Mcl-1 following H_2O_2 treatment. We have examined three independently selected clones of WT and mutant Mcl-1 and obtained essentially the same results in independent clones (data not shown). These data indicated that eliminating phosphorylation sites increased anti-apoptotic activity of Mcl-1. In other words, Mcl-1 appears to be negatively regulated through phosphorylation of Ser-121 and Thr-163 by JNK following H_2O_2 stimulation.

DISCUSSION

In this study, we demonstrated that Mcl-1 was phosphorylated at Ser-121 and Thr-163 through the JNK pathway and inactivated following H_2O_2 treatment. We also demonstrated that both JNK and p38 could phosphorylate Mcl-1 *in vitro*, whereas ERK induced little phosphorylation. A recent study also suggested using an ERK inhibitor that ERK was involved in 12-*O*-tetradecanoylphorbol-13-acetate-induced Mcl-1 phosphorylation (33). Further investigations will be needed to determine whether the ERK pathway is also involved in Mcl-1 phosphorylation depending on stimuli.

We identified two phosphorylation sites, which regulate the anti-apoptotic function of Mcl-1 in response to H_2O_2. Although human Mcl-1 possesses five potential phosphorylation sites that can be phosphorylated by JNK and p38, we could not detect any phosphorylation in the S121A/T163A mutant, sug-

gesting that Ser-121 and Thr-163 are the main sites to undergo H_2O_2-induced phosphorylation. Bcl-2 has been shown to be phosphorylated by JNK in at least four serine/threonine sites. Especially, Ser-70 and Ser-87 play an important role in negatively regulating the anti-apoptotic function of Bcl-2 (9, 11). Recent work suggested that the number of phosphorylated sites of Bcl-2 appeared to depend on the intensity of kinase activation. We detected another shift of gel mobility of the S121A/T163A mutant of Mcl-1 when it was co-expressed with JNK and ASK1ΔN in 293 cells (data not shown). It remains to be determined whether other phosphorylation sites contribute to the regulation of the anti-apoptotic activity of Mcl-1.

The mechanisms by which phosphorylation of Bcl-2 regulates anti-apoptotic function are poorly understood. Several studies have shown that phosphorylated Bcl-2 does not heterodimerize with Bax, and thus, apoptosis is promoted by an increase in the amount of free Bax (34, 35). We could not detect any changes in the interaction of Bax and Mcl-1 before or after the phosphorylation of Mcl-1 (data not shown). However, in the phosphorylation sites of Mcl-1 located in the PEST motif, there was no difference in the half-life of WT and S121A/T163A mutant of Mcl-1 after H_2O_2 stimulation (data not shown). Further studies will be needed to elucidate the mechanism of phosphorylation-mediated inactivation of Mcl-1.

The JNK signaling pathway is essential for exocytotoxic stress-induced apoptosis in neurons and UV-induced apoptosis in mouse embryonic fibroblast (8, 36). It seems that activated JNK acts on mitochondria and induces apoptosis through the release of cytochrome *c* (7, 8). The mechanism of cytochrome *c* release by JNK is not known at all. Although the Bcl-2 family is a potential target of JNK that regulates cytochrome *c*, several discrepancies have been pointed out. For example, Bcl-2 phosphorylation has been suggested to increase rather than decrease anti-apoptotic function (37). Stimuli that cause JNK-induced apoptosis such as UV do not necessarily cause Bcl-2 phosphorylation (8).

In our study, Mcl-1 was phosphorylated by JNK and its anti-apoptotic function decreased. Phosphorylation and inactivation of Mcl-1 thus may be one of the mechanisms by which JNK induces apoptosis in response to oxidative stress.

Acknowledgments—We thank Y. Tsujimoto and S. Shimizu for valuable comments. We are grateful to H. Okita for providing plasmids and antibodies. We also thank all the members of Cell Signaling Laboratory for critical comments.

REFERENCES

1. Carden, D. L., and Granger, D. N. (2000) *J. Pathol.* **190,** 255–266
2. Muller, I., Jenner, A., Bruchelt, G., Niethammer, D., and Halliwell, B. (1997) *Biochem. Biophys. Res. Commun.* **230,** 254–257
3. Guigliano, O., and Ceriello, A. (1996) *Diabetes Care* **19,** 257–267
4. Tobiume, K., Matsuzawa, A., Takahashi, T., Nishitoh, H., Morita, K., Takeda, K., Minowa, O., Miyazono, K., Noda, T., and Ichijo, H. (2001) *EMBO J.* **2,** 222–228
5. Ichijo, H., Nishida, E., Irie, K., ten Dijke, P., Saitoh, M., Moriguchi, T., Takagi, M., Matsumoto, K., Miyazono, K., and Gotoh, Y. (1997) *Science* **275,** 90–94
6. Saitoh, M., Nishitoh, H., Fujii, M., Takeda, K., Tobiume, K., Sawada, Y., Kawabata, M., Miyazono, K., and Ichijo, H. (1998) *EMBO J.* **17,** 2596–2606
7. Hatai, T., Matsuzawa, A., Inoshita, S., Mochida, Y., Kuroda, T., Sakamaki, K., Kuida, K., Yonehara, S., Ichijo, H., and Takeda, K. (2000) *J. Biol. Chem.* **275,** 26576–26581
8. Tournier, C., Hess, P., Yang, D. D., Xu, J., Turner, T. K., Nimnual, A., Bar-Sagi, D., Jones, S. N., Flavell, R. A., and Davis, R. J. (2000) *Science* **288,** 870–874
9. Yamamoto, K., Ichijo, H., and Korsmeyer, S. J. (1999) *Mol. Cell. Biol.* **19,** 8469–8478
10. Maundrell, K., Antonsson, B., Magnenat, E., Camps, M., Muda, M., Chabert, C., Gillieron, C., Boschert, U., Vial-Knecht, E., Martinou, J. C., and Arkinstall, S. (1997) *J. Biol. Chem.* **272,** 25238–25242
11. Thomas, A., Giesler, T., and White, E. (2000) *Oncogene* **19,** 5259–5269
12. Ojala, P. M., Yamamoto, K., Castanos-Velez, E., Biberfeld, P., Korsmeyer, S. J., and Makela, T. P. (2000) *Nat. Cell Biol.* **2,** 819–825
13. Kozopas, K. M., Yang, T., Buchan, H. L., Zhou, P., and Craig, R. W. (1993) *Proc. Natl. Acad. Sci. U. S. A.*, **90,** 3516–3520
14. Umezawa, A., Maruyama, T., Inazawa, J., Imai, S., Takano, T., and Hata, J. (1996) *Cell Struct. Funct.* **21,** 143–150
15. Shigemasa, K., Katoh, O., Shiroyama, Y., Mihara, S., Mukai, K., Nagai N., and Ohama, K. (2002) *Jpn. J. Cancer Res.* **93,** 542–550
16. Zhang, B., Gojo, I., and Fenton, R. G. (2002) *Blood* **99,** 1885–1893
17. Zhou, P., Levy, N. B., Xie, H., Qian, L., Lee, C. Y., Gascoyne, R. D., and Craig, R. W. (2001) *Blood* **97,** 3902–3909
18. Yang, T., Kozopas, K. M., and Craig, R. W. (1995) *J. Cell Biol.* **128,** 1173–1184
19. Bodrug, S. E., Aime-Sempe, C., Sato, T., Krajewski, S., Hanada, M., and Reed, J. C. (1995) *Cell Death Differ.* **2,** 173–182
20. Townsend, K. J., Trusty, J. L., Traupman, M. A., Eastman, A., and Craig, R. W. (1998) *Oncogene* **17,** 1223–1234
21. Townsend, K. J., Zhou, P., Qian, L., Bieszczad, C. K., Lowrey, C. H., Yen, A., and Craig, R. W. (1999) *J. Biol. Chem.* **274,** 1801–1813
22. Wang, J. M., Chao, J. R., Cen, W., Kuo, M. L., Yen, J. J., and Yang-Yen, H. F. (1999) *Mol. Cell. Biol.* **19,** 6195–6206
23. Zhou, P., Qian, L., Kozopas, K. M., and Craig, R. W. (1997) *Blood* **89,** 630–643
24. Reynolds, J. E., Li, J., and Craig, R. W. (1996) *Exp. Cell Res.* **225,** 430–436
25. Reynolds, J. E., Yang, T., Qian, L., Jenkinson, J. D., Zhou, P., Eastman, A., and Craig, R. W. (1994) *Cancer Res.* **54,** 6348–6352
26. Nishitoh, H., Saitoh, M., Mochida, Y., Takeda, K., Nakano, H., Rothe, M., Miyazono, K., and Ichijo, H. (1998) *Mol. Cell* **2,** 389–395
27. Morita, K., Saitoh, M., Tobiume, K., Matsuura, H., Enomoto, S., Hideki Nishitoh, H., and Ichijo, H. (2001) *EMBO J.* **20,** 6028–6036
28. Matsuura, H., Nishitoh, H., Takeda, K., Matsuzawa, A., Amagasa, T., Ito, M., Yoshioka, K., and Ichijo, H. (2002) *J. Biol. Chem.* **277,** 40703–40709
29. Saito, I., Oya, Y., Yamamoto, K., Yuasa, T., and Shimojo, H. (1985) *J. Virol.* **54,** 711–719
30. Miyake, S., Makimura, M., Kanegae, Y., Harada, S., Sato, Y., Takamori, K., Tokuda, C., and Saito, I. (1996) *Proc. Natl. Acad. Sci. U. S. A.* **93,** 1320–1324
31. Guyton, K. Z., Liu, Y., Gorospe, M., Xu, Q., and Holbrook, N. J. (1996) *J. Biol. Chem.* **271,** 4138–4142
32. Chang, B. S., Minn, A. J., Muchmore, S. W., Fesik, S. W., and Thompson, C. B. (1997) *EMBO J.* **16,** 968–977
33. Domina, A. M., Smith, J. H., and Craig, R. W. (2000) *J. Biol. Chem.* **275,** 21688–21694
34. Basu, A., and Haldar, S. (1998) *Int. J. Oncol.* **13,** 659–664
35. Haldar, S., Basu, A., and Croce, C. M. (1998) *Cancer Res.* **58,** 1609–1615
36. Yang, D. D., Kuan, C. Y., Whitmarsh, A. J., Rincon, M., Zheng, T. S., Davis, R. J., Rakic, P., and Flavell, R. A. (1997) *Nature* **389,** 865–870
37. Ito, T., Deng, X., Carr, B., and May, W. S. (1997) *J. Biol. Chem.* **272,** 11671–11673

Bone Marrow–Derived Regenerated Cardiomyocytes (CMG Cells) Express Functional Adrenergic and Muscarinic Receptors

Daihiko Hakuno, MD, PhD; Keiichi Fukuda, MD; Shinji Makino, MD; Fusako Konishi, PhD; Yuichi Tomita, MD; Tomohiro Manabe, MD; Yusuke Suzuki, MD; Akihiro Umezawa, MD, PhD; Satoshi Ogawa, MD, PhD

Background—We recently reported that cardiomyocytes could be differentiated from bone marrow mesenchymal stem cells in vitro by 5-azacytidine treatment. In native cardiomyocytes, adrenergic and muscarinic receptors play crucial roles in mediating heart rate, conduction velocity, contractility, and cardiac hypertrophy. We investigated whether these receptors are expressed in differentiated CMG cells, and if so, whether they have downstream signaling systems.

Methods and Results—Reverse transcription–polymerase chain reaction revealed that CMG cells had already expressed α_{1A}-, α_{1B}-, and α_{1D}-adrenergic receptor mRNA before 5-azacytidine treatment, whereas expression of β_1-, β_2-adrenergic and M_1-, M_2-muscarinic receptors was first detected at 1 day. Phenylephrine dose-dependently induced phosphorylation of ERK1/2, which was completely inhibited by prazosin, and significantly increased cell size. Isoproterenol augmented cAMP by 38-fold, which was fully inhibited by propranolol. Isoproterenol (10^{-7} mol/L) increased the spontaneous beating rate by 47.6% (basal, 127±16 bpm), and propranolol and CGP20712A (β_1-selective blocker) reduced it by 79.0% and 71.0%, respectively, whereas ICI118551 (β_2-selective blocker) induced slight reduction. Cell motion, percent shortening, and contractile velocity were increased by 37.5%, 26.9%, and 50.6%, respectively, in response to isoproterenol. Phenylephrine and isoproterenol augmented ANP and BNP gene expressions. Carbachol increased IP_3 by 32-fold, which was markedly inhibited by atropine as well as AFDX116 (M_2-selective blocker) measured by radioimmunoassay.

Conclusions—These findings indicate that CMG cells expressed α_{1A}, α_{1B}, and α_{1D} receptors before differentiation and expressed β_1, β_2, M_1, and M_2 receptors after they obtained the cardiomyocyte phenotype. These receptors had functional signal transduction pathways and could modulate cell function. (***Circulation.*** **2002;105:380-386.)**

Key Words: cells ■ heart rate ■ receptors, adrenergic, beta ■ signal transduction ■ receptors, adrenergic, alpha

A growing body of evidence shows that neurohumoral factors strongly modify heart rate, conduction velocity, myocardial contractility, and hypertrophy in cardiomyocytes.[1-3] The sympathetic and parasympathetic nerves play a critical role in modulating these cardiac functions through α_1-, β_1-, and β_2-adrenergic and muscarinic receptors. α_1-Adrenergic receptor agonists strongly induce cardiac hypertrophy both in vivo and in vitro.[4,5] There are 3 α_1-receptor subtypes, α_{1A}, α_{1B}, and α_{1D}, all of which are expressed in the heart.[6] The α_{1A} and α_{1B} subtypes are abundant in adult rat cardiomyocytes, but specific functional differences of each receptor remain unknown. There are 3 known subtypes of β-adrenergic receptors: β_1, β_2, and β_3.[7] Cardiomyocytes express β_1 and β_2 receptors, and β_1 receptors play a pivotal role in mediating heart rate, conduction velocity, and contractility.[7,8]

Muscarinic receptors mediate postganglionic parasympathetic cholinergic signal transduction and have 5 subtypes; M_1 through M_5.[9] Cardiomyocytes mainly express the M_2-receptor subtype, and this receptor is crucial to the negative regulation of heart rate, conduction velocity, and contractility.[9] Sharma et al[10] showed that M_1 receptors are also expressed in adult ventricular cardiomyocytes and increase the magnitude of calcium transients. Although the precise function of the M_1 receptor remains unknown, it may be able to modulate the function of cardiomyocytes.

A number of studies have demonstrated that cardiomyocytes can be differentiated from various multipotent stem cells such as embryonic stem (ES) cells[11] and embryonic carcinoma cells.[12] We recently reported that cardiomyocytes could be generated from bone marrow mesenchymal stem cells in vitro with the use of 5-azacytidine (5-AZ).[13] These CMG cells showed spontaneous beating and expressed atrial natriuretic peptide (ANP) and brain natriuretic peptide (BNP). Analysis of the isoforms of contractile proteins revealed that CMG cells had a fetal ventricular phenotype.

Received August 15, 2001; revision received November 7, 2001; accepted November 8, 2001.

From the Cardiopulmonary Division (D.H., K.F., S.M., F.K., Y.T., T.M., Y.S., S.O.), Department of Internal Medicine, Institute for Advanced Cardiac Therapeutics (K.F.), and the Department of Pathology (A.U.), Keio University School of Medicine, Tokyo, Japan.

Correspondence to Keiichi Fukuda, MD, PhD, Institute for Advanced Cardiac Therapeutics, Keio University School of Medicine, 35 Shinanomachi, Shinjuku-ku, Tokyo 160-8582, Japan. E-mail:kfukuda@sc.itc.keio.ac.jp

Circulation is available at http://www.circulationaha.org

TABLE 1. PCR Primers Used in Study

	Sense Primers	Antisense Primers
α_{1A}	GAGAATTCCGAGGCCTCAAGTCCGGCCT	TTGAATTCTCGGGAAAACTTGAGCAG
α_{1B}	CTGGGGAGAGTTGAAAGATGCC	CCGACAGGATGACCAAGATGTT
α_{1D}	TTGAATTCCTACAGAGACCCACGACCCAG	CGGAATTCTTAAATGTCAGTCTCCCGGAG
β_1	ACGCTCACCAACCTCTTCAT	AGGGGCACGTAGAAGGAGAC
β_2	CCTCATGTCGGTTATCGTCC	GGCACGTAGAAAGACACAATC
M_1	CTGGTTTCCTTCGTTCTCTG	GCTGCCTTCTTCTCCTTGAC
M_2	GGCAAGCAAGAGTAGAATAAA	GCCAACAGGATAGCCAAGATT
ANP	TTGGCTTCCAGGCCATATTG	AAGAGGGCAGATCTATCGGA
BNP	ATGGATCTCCTGAAGGTGCT	TCTTGTGCCCAAAGCAGCTT
GAPDH	AGTATGACTCCACTCACGGCAA	TCTCGCTCCTGGAAGATGGT

Furthermore, CMG cells expressed Nkx2.5, GATA-4, TEF-1, and MEF-2C before 5-AZ treatment and expressed other cardiac-specific transcription factors such as MEF-2A and MEF-2D and developed a cardiomyocyte phenotype after the treatment, suggesting that the developmental process of CMG cells was close to that of cardiomyoblasts.

These regenerated cardiomyocytes could be a useful and powerful tool for cardiomyocyte transplantation, but first further characterization of their cardiomyocyte phenotype is needed. Since adrenergic receptors and muscarinic receptors are critically implicated in modulating cardiac function, we determined whether these receptors are expressed in CMG cells, and if so, whether they are functional. We report that differentiated CMG cells expressed α_{1A}-, α_{1B}-, α_{1D}-, β_1-, and β_2-adrenergic receptors and muscarinic M_1 and M_2 receptors and that stimulation of CMG cells with phenylephrine, isoproterenol, or carbachol could activate downstream signaling pathways through specific receptors.

Methods

Cell Culture and 5-AZ Treatment

Cells were cultured on 60-mm dishes in Iscove's Modified Dulbecco's Medium (GIBCO BRL) as described.[13] To induce differentiation, cells were treated with 3 μmol/L of 5-AZ for 24 hours and were maintained for several weeks. The percentage of the cardiomyocytes after 5-AZ was approximately 20% to 30%, the same as described previously.[13] The CMG cardiomyocytes began to spontaneously contract 2 to 3 weeks after 5-AZ treatment.

Reverse Transcription–Polymerase Chain Reaction Analysis

Total RNA was extracted, and reverse transcription–polymerase chain reaction (RT-PCR) was performed as described.[13] The expressions of α_{1A}, α_{1B}, α_{1D}, β_1, β_2, M_1, and M_2 receptors, ANP, and BNP mRNAs were analyzed. PCR was performed for 30 to 40 cycles, with each cycle consisting of denaturation at 94°C, annealing at 54°C to 60°C, and amplification at 72°C for 1 minute each. The PCR primers used are listed in Table 1. Before quantitative analysis, the linear range of the PCR cycles was measured for each receptor, and the appropriate number of PCR cycles was determined. Densitometric analysis was applied to quantify mRNA levels. GAPDH was used as an internal control for each sample.

Western Blot Analysis

Polyclonal antibodies to extracellular responsive kinase (ERK)1 and phosphorylated ERK1/2 were purchased from Santa Cruz Biotechnology and New England Biolabs, respectively. Western blot analysis was performed as described previously.[14]

Immunostaining and Cell Sizing Protocol

Monoclonal antibody (MF20) to sarcomeric myosin was obtained from ATCC. Immunostaining and measurement of cell size (cell area, perimeter) were performed as described previously.[13,14]

cAMP Accumulation Assays

Cells were incubated in serum-free medium with 10^{-4} mol/L of 3-isobutyl-1-methylxanthine (Sigma) for 30 minutes and stimulated with isoproterenol (Sigma) for 10 minutes. The medium was aspirated rapidly, and incubation was terminated by addition of 1 mL of ice-cold 0.1N HCl. The lysates were centrifuged at 3000 rpm for 10 minutes, and the supernatants were used as samples. The cAMP levels were counted by radioimmunoassay with the assay kit (YAMASA).

Videotape Recording

The cultured cells were observed through an inverted-type phase-contrast video microscope (IX70, OLYMPUS) equipped with a ×4 quartz objective lens and a ×1 relay lens as described.[13] Contractile parameters (cell motion distance, percent shortening, and contractile velocity) were analyzed by NIH image. Measurements of changes in cell length are not possible in CMG cells because they lack a single axis of myofibrillar alignment. Therefore, cell shortening diameter was calculated in the individual cells.

Inositol Triphosphate Production Assays

Cells were incubated in serum-free medium for 1 hour and were incubated in serum-free medium containing 10 mmol/L LiCl for 30 minutes.[15] Stimulation was terminated by aspiration of medium and addition of 400 μL of ice-cold 20% perchloric acid for 20 minutes. The lysates were centrifuged at 5000 rpm, and the supernatants were titrated to pH 7.5 with 1.5N KOH. Then, they were centrifuged at 5000 rpm for 15 minutes at 4°C, and the supernatants were used as samples. Inositol triphosphate (IP_3) production was measured by radioimmunoassay with an assay kit (Amersham).

Statistical Analysis

Values are presented as mean±SEM. The significance of differences among mean values was determined by ANOVA. Statistical comparison of the control group with the treated group was carried out by means of the nonparametric Fisher's multiple comparison tests. The accepted level of significance was $P<0.05$.

Results

CMG Cells Express α_1-Adrenergic Receptor mRNA Before Final 5-AZ Treatment

To begin to address whether α_1-adrenergic receptors were involved in modulating the function of CMG cells, we first

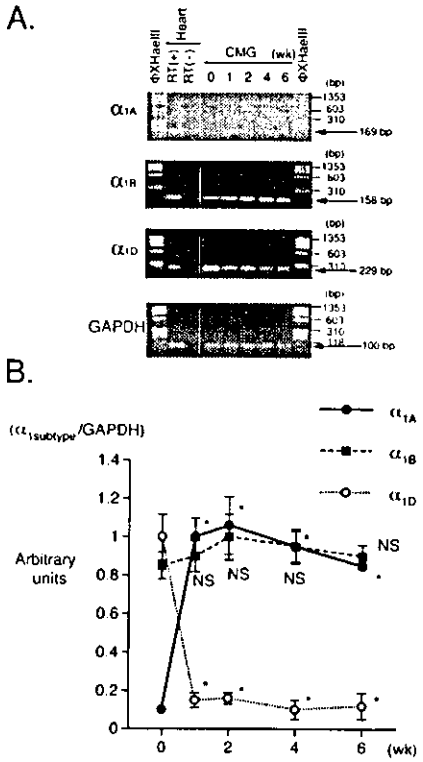

Figure 1. Temporal expression of α_1-adrenergic receptor subtype mRNA in CMG cells. A, Each panel shows RT-PCR products for α_{1A}, α_{1B}, and α_{1D} receptors and GAPDH. ΦXHaeIII is a DNA size marker. Heart indicates adult murine left ventricles; RT (+) or RT(−), with or without reverse transcription and indicates positive or negative control; and Wk, weeks. B, Densitometric analysis was performed; ratio of RT-PCR product of α_1 subtype to that of GAPDH is shown. Data were obtained from 5 separate experiments and were presented as arbitrary units over controls. Values are mean±SEM. *$P<0.01$ vs controls (before 5-AZ treatment).

detected α_1 receptor expression (Figure 1A). Adult murine ventricles were used as a positive control. CMG cells expressed all the α_1 receptor subtypes (α_{1A}, α_{1B}, and α_{1D}) before 5-AZ treatment. A low level of expression of α_{1A} was observed before 5-AZ treatment, but their expression was markedly augmented after the treatment. Expression of α_{1B} was unaffected by the treatment. A high level of expression of α_{1D} was first detected before 5-AZ treatment, but it noticeably decreased after the treatment. The quantitative analysis of their expression is shown in Figure 1B.

Phenylephrine Induces Activation of ERK1/2 and Hypertrophy Through α_1-Receptors in CMG Cells

To investigate whether α_1 receptors are expressed at the protein level and can transduce signals, we stimulated CMG cells with phenylephrine (Sigma) and detected phosphorylation of ERK1/2. Phenylephrine induced phosphorylation of ERK1/2 in a time- and dose-dependent manner in the cells at 2 weeks after 5-AZ treatment (Figure 2, A and B). ERK1/2 was activated as early as 5 minutes and peaked at 10 minutes. Similar results were also obtained before 5-AZ treatment (data not shown). We preincubated the cells with prazosin (Sigma) before the stimulation and measured the phosphorylation in cells before and at 2 weeks after 5-AZ treatment.

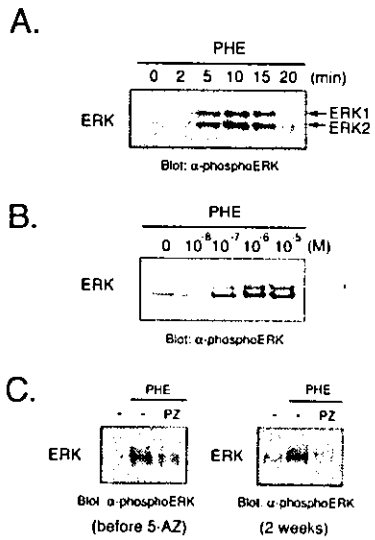

Figure 2. Effect of phenylephrine (PHE) on phosphorylation of ERK1/2 in CMG cells. A, Cells at 2 weeks after 5-AZ treatment were stimulated with phenylephrine (10^{-4} mol/L), and Western blot analysis was performed to detect phosphorylation of ERK1/2. Similar results were obtained in 3 separate experiments. B, Cells were stimulated with phenylephrine (10^{-8} - 10^{-5} mol/L) for 10 minutes, and phosphorylation of ERK was detected. Results were reproducible in 3 separate experiments. C, Prazosin (PZ) (10^{-6} mol/L) was added to cells 20 minutes before stimulation with phenylephrine (10^{-6} mol/L). Left panel shows results in CMG cells before 5-AZ treatment. Right panels show that of CMG cells at 2 weeks after 5-AZ treatment. We obtained similar results in 3 separate experiments.

Phenylephrine-induced phosphorylation was completely inhibited by prazosin (Figure 2C). Next, we investigated whether phenylephrine is capable of inducing CMG cell hypertrophy. Phenylephrine increased the cell area and perimeter by 42.2% and 24.5%, respectively, over controls. These findings indicated that CMG cells expressed functionally active α_1-adrenergic receptors.

CMG Cells Express β_1- and β_2-Adrenergic Receptor mRNA After 5-AZ Treatment

β_1- and β_2-adrenergic receptors play a crucial role in catecholamine-induced increases in heart rate, conduction velocity, and contractility.[7,10] To explore whether β_1 and β_2 receptors are functional, we examined their expression. CMG cells did not express their transcripts before 5-AZ treatment. They expressed β_1 and β_2 receptor mRNA from 1 day onward after treatment by PCR level and were stable after 1 week (Figure 3A). Quantitative analysis is shown in Figure 3B. The temporal expression pattern of these receptors was different from that of α_1. These findings suggest that CMG cells express β_1 and β_2 mRNA when they attain the cardiomyocyte phenotype.

Isoproterenol Increases cAMP Content, Spontaneous Beating Rate, and Contractility in CMG Cells

To examine whether β_1 and β_2 receptors can transduce their signals in CMG cells, we stimulated the cells with various concentrations of isoproterenol and measured intracellular

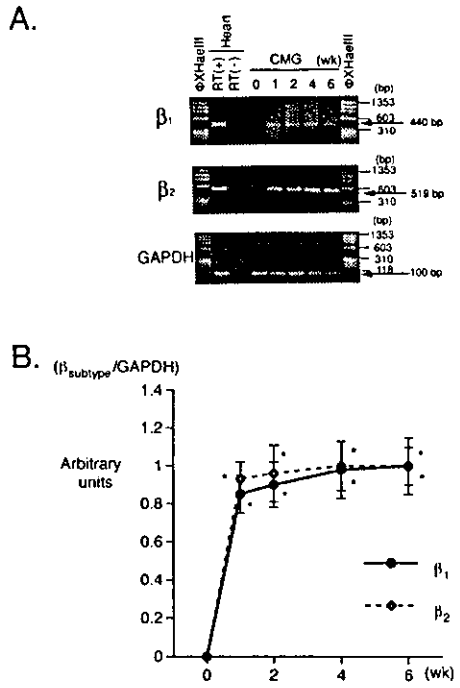

Figure 3. Temporal expression of β_1- and β_2-adrenergic receptor mRNA in CMG cells. A, Experiments were run as described in Figure 1A. Each panel shows RT-PCR products of β_1, β_2 receptors and GAPDH. B, Densitometric analysis was performed; ratio of the RT-PCR product of β subtype to that of GAPDH is shown. Data were obtained from 5 separate experiments and were presented as arbitrary units over controls. *$P<0.01$ vs controls.

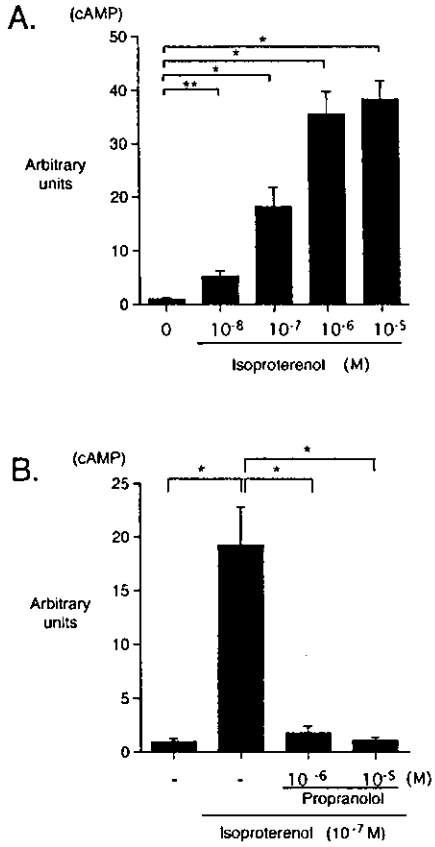

Figure 4. β-Receptor-mediated cAMP accumulation in CMG cells. A, Effect of isoproterenol on cAMP accumulation in CMG cells at 2 weeks after 5-AZ treatment. B, Cells were preincubated with propranolol (10^{-6} or 10^{-5} mol/L) for 20 minutes and stimulated with isoproterenol (10^{-7} mol/L) for 10 minutes. Data were obtained from 5 separate experiments and were presented as arbitrary units over the controls. *$P<0.01$, **$P<0.05$ vs controls.

cAMP content. Isoproterenol increased cAMP in a dose-dependent manner (Figure 4A). The absolute cAMP values of controls and cells stimulated with 10^{-7} mol/L of isoproterenol were 8.1 ± 1.5 and 147.4 ± 16.2 pmol/10^5 cells, respectively. cAMP increased by 38-fold with isoproterenol over the control. We next preincubated the cells with propranolol (Sigma) and stimulated with isoproterenol. Propranolol completely inhibited isoproterenol-induced cAMP accumulation (Figure 4B). These findings demonstrated that CMG cells not only expressed β_1- and β_2-adrenergic receptor protein but also expressed the signal transduction molecules for these receptors.

To ascertain whether isoproterenol could increase the spontaneous beating rate, we stimulated the cells with isoproterenol and observed them for changes in beating rate (Table 2). The beating rate of the control cells ranged from 58 to 292 (average 127 ± 16, n=100) beats/min. The spontaneous beating rate increased significantly by 47.6% with isoproterenol. In some cells, however, isoproterenol did not increase the beating rate. Next, the cells were preincubated with either vehicle (PBS), propranolol, CGP20712A (β_1-selective blocker, RBI-Sigma), or ICI118551 (β_2-selective blocker, Sigma)[17] and were stimulated with isoproterenol. Propranolol, CGP20712A, and ICI118551 reduced isoproterenol-induced increase in beating rate by 79.0%, 71.0%, and 21.0%, respectively.

We further investigated the effect of isoproterenol on the contractile function. Isoproterenol increased the cell motion distance, percent shortening, and contractile velocity by 37.5%, 26.9%, and 50.6%, respectively. Isoproterenol-induced increase in contractility was almost completely inhibited by both propranolol and CGP20712A. Collectively, these results indicated that β_1- and β_2-adenergic receptors expressed in CMG cells were functional and that the isoproterenol-induced increase in spontaneous beating rate and contractility might be mediated mainly by β_1 receptors.

Phenylephrine and Isoproterenol Induce ANP and BNP mRNA Expression

Hypertrophic stimuli are well known to induce the reprogramming of gene expression in cardiomyocytes. To investigate whether these stimuli can induce cardiac hypertrophy marker gene expression, we performed RT-PCR to quantify mRNA expression of ANP and BNP. Each value was normalized with GAPDH. Both phenylephrine (5×10^{-5} mol/L) and isoproterenol (10^{-4} mol/L) significantly induced the ANP (24 hours) gene by 5.1- and 6.9-fold, respectively. They also induced the BNP (1 hour) gene by 5.1- and 3.8-fold, respectively. These findings demonstrated CMG cells to have functional α- and β-adrenergic signal transduction systems.

TABLE 2. Isoproterenol Increases Spontaneous Beating Rate and Contractility of CMG Cells, Mainly Through β_1 Receptors

		Isoproterenol, 10^{-7} mol/L			
	Control	Vehicle	Propranolol, 10^{-7} mol/L	CGP20712A, 10^{-7} mol/L	ICI118551, 10^{-7} mol/L
% Increase in beating rate	...	47.6±8.4*	10.0±1.9†	13.8±2.4†	37.6±1.9‡
Cell motion, μm	5.0±0.3	6.8±0.7*	5.6±0.8‡	5.3±0.6‡	ND
% Shortening, %	6.9±0.5	8.5±1.2*	7.2±0.8‡	5.6±0.6‡	ND
Contractile velocity, μm/s	71.1±5.2	100.9±11.0*	71.3±8.8‡	70.6±6.6‡	ND

CMG cells at 4 weeks after 5-AZ treatment were initially exposed to prazosin (10^{-6} mol/L) for 30 minutes to block α_1-adrenergic receptors. Cells were preincubated for 20 minutes with either vehicle (PBS), propranolol, CGP20712A, or ICI118551, and then stimulated with isoproterenol. Beating rate was counted at 3 minutes after stimulation. Contractile parameters were analyzed at 90 seconds after stimulation. For contractile parameters, each value was calculated as the mean of 3 randomly selected beats in one cell. PBS was added to control.

Values are mean±SEM (n=100, each). ND, Not determined.

*$P<0.05$ vs control, †$P<0.01$ vs vehicle (isoproterenol only), ‡$P<0.05$ vs vehicle.

CMG Cells Express Muscarinic Receptor mRNA After 5-AZ Treatment

To date, 5 subtypes (M_1 through M_5) of muscarinic receptors have been cloned.[9] M_1 and M_2 receptor subtypes are expressed in murine neonatal and adult cardiomyocytes.[10] Figure 5A shows the temporal expression pattern of M_1 and M_2 receptor mRNA. Neither receptor was detected before 5-AZ treatment. CMG cells began to express both receptors 1 day after the treatment by PCR level, and their expression became stable after 1 week. Quantitative analysis of their expression is shown in Figure 5B. These findings showed that the M_1 and M_2 receptors are expressed when they obtain the cardiomyocyte phenotype.

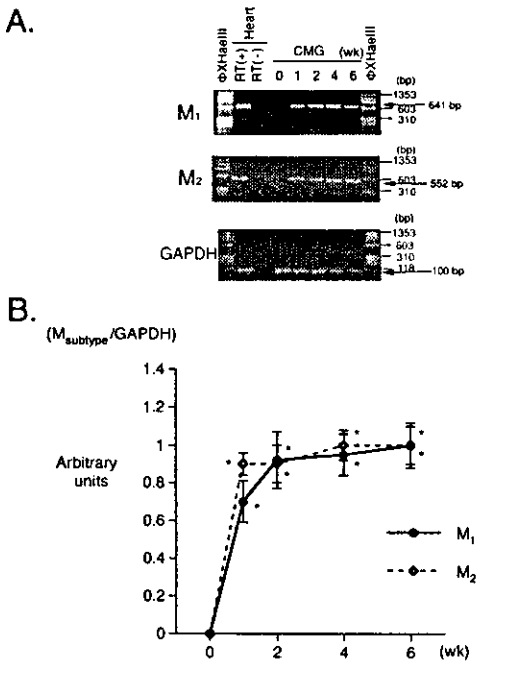

Figure 5. Temporal expression of M_1 and M_2 muscarinic receptor mRNA in CMG cells. A, Each panel shows RT-PCR products of M_1, M_2 receptors and GAPDH. B, Densitometric analysis was performed; ratio of the RT-PCR product of muscarinic subtype to that of GAPDH is shown. Data were obtained from 5 separate experiments and were presented as arbitrary units over controls. *$P<0.01$ vs controls.

Carbachol Stimulates IP_3 Production Through Muscarinic Receptors in CMG Cells

To explore whether these muscarinic receptors can transduce signals, we stimulated CMG cells with the muscarinic receptor agonist carbachol (Calbiochem) for 5 minutes and measured intracellular IP_3 content. Carbachol increased IP_3 content in a dose-dependent manner (Figure 6A). The absolute IP_3 values of the controls and the cells stimulated with 10^{-7} mol/L of carbachol were 0.4±0.1 and 13.0±1.2 pmol/10^5 cells, respectively. IP_3 content peaked by 32-fold over the control cells. We then preincubated the cells with atropine and the M_2-selective blocker AFDX116 (Tocris Cookson) for 5 minutes, stimulated with carbachol. Atropine and AFDX116 inhibited carbachol-induced IP_3 production by 84.5% and 89.2%, respectively (Figure 6B). These findings indicate that muscarinic receptors can transduce signals and that M_2 receptors play a critical role in this carbachol-induced IP_3 production.

Discussion

α_1-Adrenergic Receptor Expression in CMG Cells

The present study demonstrates that bone marrow–derived CMG cardiomyocytes express all the α_1-receptor subtypes (α_{1A}, α_{1B}, and α_{1D}) before the final 5-AZ treatment and consistently express thereafter. Moreover, phenylephrine induced ERK activation and hypertrophy in CMG cells, which was inhibited by prazosin. We supposed that expression of these α_1-receptor subtypes in undifferentiated CMG cells might be explained by their ubiquitous or wide expression in vivo.[6] Interestingly, the present results show that expression of α_{1A} receptors gradually increase, whereas that of α_{1D} receptors prominently decrease after 5-AZ treatment. This transcriptional switch might result from the fact that CMG cells obtain the cardiomyocyte phenotype. Stewart et al[18] showed α_{1A} and α_{1B} receptor mRNA to be expressed abun-

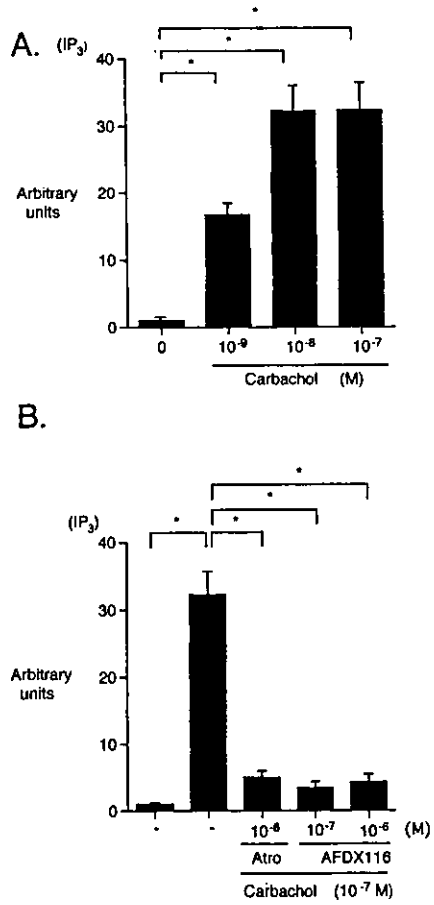

Figure 6. Carbachol induced IP_3 production through M_2-muscarinic receptors in CMG cells. A, Effect of carbachol on IP_3 production in CMG cells at 2 weeks after 5-AZ treatment. B. Effect of atropine (ATRO) (10^{-6} mol/L) and AFDX116 (10^{-7} or 10^{-6} mol/L) on carbachol-induced IP_3 production. Data were obtained from 5 separate experiments and were presented as arbitrary units over controls. *$P<0.01$ vs controls.

dantly in both neonatal and adult rat hearts, whereas α_{1D} receptors were expressed only at a low level. They also reported that hypertrophic stimuli induced an increase in α_{1A} and a decrease in α_{1D} receptors.[19] Thus, temporal changes in the expression of the α_1-adrenergic receptor subtype in CMG cells are very similar to the postnatal changes previously observed in the neonatal rat heart.

β_1- and β_2-Adrenergic Receptor Expression in CMG Cells

Cardiomyocytes express both β_1- and β_2-adrenergic receptors in mammalian hearts, the β_1 receptor being the predominant subtype (approximately 75% to 80% of total β receptors) [7]. We demonstrated that CMG cells first express both β_1 and β_2 receptors on 1 day when directed to differentiate into the cardiomyocyte and that stimulation of β receptors with isoproterenol dose-dependently increases their cAMP content, which is completely blocked by propranolol. In CMG cells, the dose-response curve of cAMP accumulation by isoproterenol is similar to that in neonatal rat[17] cardiomyocytes. These findings indicate that differentiated CMG cells have functionally active β receptors. Heart-specific expression of β_1 receptors is in accordance with the temporal expression of their mRNA in CMG cells.

We observed that isoproterenol had a positive chronotropic effect on CMG cells. The increment in beating rate (47.6%) is similar to that of adult murine cardiomyocytes (≈65%)[20] and ES cell–derived cardiomyocytes (≈40%).[11] CGP20712A significantly inhibited isoproterenol-induced increase in beating rate to the same extent as the nonselective β-blocker propranolol. However, ICI118551 slightly inhibited this increase. These results suggest that the β_1 receptor was the predominant subtype to mediate changes in beating rate in CMG cells. Moreover, contractility represented as cell motion, percent shortening, and contractile velocity was significantly augmented in response to isoproterenol. This positive inotropic effect was completely inhibited by propranolol as well as CGP20712A. To our knowledge, this is the first report to show the changes in contractility in regenerated cardiomyocytes. The increase in cell motion, percent shortening, and contractile velocity in CMG cells in response to isoproterenol were similar to those of neonatal rat cardiomyocyte.[17] These findings confirmed that the β_1 receptors played a critical role to mediate isoproterenol-induced signaling in differentiated CMG cells.

M_1- and M_2-Muscarinic Receptor Expression in CMG Cells

Muscarinic receptors show tissue-specific expression, and cardiomyocytes mainly express M_2 receptors in mouse and human.[21] We found that both M_1 and M_2 muscarinic receptor mRNA was first expressed in CMG cells after 5-AZ treatment and that carbachol increased IP_3 production in a dose-dependent manner, which was markedly inhibited by atropine and AFDX116. Since the localization of muscarinic receptors is tissue-specific, it does not seem surprising that these receptors were expressed when they were directed to differentiate into cardiomyocytes, in the same pattern as β_1- and β_2-adrenergic receptors. Previous studies showed that M_1 receptors coupled to Gq/G11 and activated phospholipase Cβ through Gqα, leading to IP_3 production, and that M_2 receptors coupled to Gi/G0/Gz and activated phospholipase Cβ through Gi$\beta\gamma$, leading to IP_3 production.[22–24] The marked inhibition of IP_3 production by AFDX116 strongly suggested that the M_2 receptor is the predominant subtype in CMG cells.

Significance of Expression of Adrenergic and Muscarinic Receptors in CMG Cells

Cardiomyocytes in vivo respond to both sympathetic and parasympathetic nerves and change heart rate, conduction velocity, and contractility, enabling them to adapt to rapid changes in systemic oxygen demand. To date and to our knowledge, the only possible candidates for regeneration of cardiomyocytes are ES cells or mesenchymal stem cell–derived CMG cells. For regenerated cardiomyocytes to be useful for transplantation, they must express functional adrenergic and muscarinic receptors. A previous pharmacological study revealed that α_1- and β_1-adrenergic and muscarinic receptors but not β_2 receptors had already contributed to chronotropic responses in early-stage (7 days) murine ES cell–derived cardiomyocytes, whereas β_2 receptors first func-

tioned at the intermediate stage (7+4 days).[11] The present study demonstrated mesenchymal stem cell–derived cardiomyocytes to express α_{1A}-, α_{1B}-, α_{1D}-, β_1-, and β_2-adrenergic and M_1- and M_2-muscarinic receptors, to maintain signal transduction pathways, and to also show cardiac hypertrophy in response to an α agonist, as well as having positive inotropic and chronotropic responses to a β agonist. In this regard, although we did not investigate all signaling pathways and their functions, CMG cells are a potential candidate for cardiomyocyte cell transplantation. Future studies are needed with the transplanted heart to analyze the adrenergic and muscarinic responses of CMG cells in vivo.

Acknowledgments

This study was supported in part by research grants (10B-1) of Nervous and Mental Disorders from the Ministry of Health and Welfare and research grants from the Ministry of Education, Science, and Culture, Japan, and Health Science Research Grants for Advanced Medical Technology from the Ministry of Welfare, Japan.

References

1. Middlekauff HR, Mark AL. The treatment of heart failure: the role of neurohumoral activation. *Intern Med.* 1998;37:112–122.
2. Prasad K, Lee P, Kalra J. Influence of endothelin on cardiovascular function, oxygen free radicals, and blood chemistry. *Am Heart J.* 1991; 121:178–187.
3. Riegger AJ. Interaction between atrial natriuretic peptide, renin system and vasopressin in heart failure. *Eur Heart J.* 1990;11(suppl B):79–83.
4. Simpson P. Norepinephrine-stimulated hypertrophy of cultured rat myocardial cells is an alpha 1 adrenergic response. *J Clin Invest.* 1983;72: 732–738.
5. Chien KR, Knowlton KU, Zhu H, et al. Regulation of cardiac gene expression during myocardial growth and hypertrophy: molecular studies of an adaptive physiologic response. *FASEB J.* 1991;5:3037–3046.
6. Alonso-Llamazares A, Zamanillo D, Casanova E, et al. Molecular cloning of alpha 1d-adrenergic receptor and tissue distribution of three alpha 1-adrenergic receptor subtypes in mouse. *J Neurochem.* 1995;65: 2387–2392.
7. Rockman HA, Koch WJ, Lefkowitz RJ. Cardiac function in genetically engineered mice with altered adrenergic receptor signaling. *Am J Physiol.* 1997;272:H1553–H1559.
8. Steinberg SF. The molecular basis for distinct beta-adrenergic receptor subtype actions in cardiomyocytes. *Circ Res.* 1999;85:1101–1111.
9. Hosey MM. Diversity of structure, signaling and regulation within the family of muscarinic cholinergic receptors. *FASEB J.* 1992;6:845–852.
10. Sharma VK, Colecraft HM, Wang DX, et al. Molecular and functional identification of m1 muscarinic acetylcholine receptors in rat ventricular myocytes. *Circ Res.* 1996;79:86–93.
11. Wobus AM, Wallukat G, Hescheler J. Pluripotent mouse embryonic stem cells are able to differentiate into cardiomyocytes expressing chronotropic responses to adrenergic and cholinergic agents and Ca^{2+} channel blockers. *Differentiation.* 1991;48:173–182.
12. Wobus AM, Kleppisch T, Maltsev V, et al. Cardiomyocyte-like cells differentiated in vitro from embryonic carcinoma cells P19 are characterized by functional expression of adrenoceptors and Ca^{2+} channels. *In Vitro Cell Dev Biol Anim.* 1994;30:425–434.
13. Makino S, Fukuda K, Miyoshi S, et al. Cardiomyocytes can be generated from marrow stromal cells in vitro. *J Clin Invest.* 1999;103:697–705.
14. Kodama H, Fukuda K, Pan J, et al. Leukemia inhibitory factor, a potent cardiac hypertrophic cytokine, activates the JAK/STAT pathway in rat cardiomyocytes. *Circ Res.* 1997;81:656–663.
15. Kovacs I, Yamamura HI, Waite SL, et al. Pharmacological comparison of the cloned human and rat M2 muscarinic receptor genes expressed in the murine fibroblast (B82) cell line. *J Pharmacol Exp Ther.* 1998;284: 500–507.
16. Hilal-Dandan R, Kanter JR, Brunton LL. Characterization of G-protein signaling in ventricular myocytes from the adult mouse heart: differences from the rat. *J Mol Cell Cardiol.* 2000;3:1211–1221.
17. Kuznetsov V, Pak E, Robinson RB, et al. Beta 2-adrenergic receptor actions in neonatal and adult rat ventricular myocytes. *Circ Res.* 1995; 76:40–52.
18. Stewart AF, Rokosh DG, Simpson PC, et al. Cloning of the rat alpha 1C-adrenergic receptor from cardiac myocytes. alpha 1C, alpha 1B, and alpha 1D mRNAs are present in cardiac myocytes but not in cardiac fibroblasts. *Circ Res.* 1994;75:796–802.
19. Rokosh DG, Stewart AF, Simpson PC, et al. Alpha1-adrenergic receptor subtype mRNAs are differentially regulated by alpha1-adrenergic and other hypertrophic stimuli in cardiac myocytes in culture and in vivo. Repression of alpha1B and alpha1D but induction of alpha1C. *J Biol Chem.* 1996;271:5839–5843.
20. Lu S, Hoey A. Changes in function of cardiac receptors mediating the effects of the autonomic nervous system in the muscular dystrophy (MDX) mouse. *J Mol Cell Cardiol.* 2000;32:143–152.
21. Sharma VK, Colecraft HM, Rubin LE, et al. Does mammalian heart contain only the M2 muscarinic receptor subtype? *Life Sci.* 1997;60: 1023–1029.
22. Nakamura F, Kato M, Kameyama K, et al. Characterization of Gq family G proteins GL1 alpha (G14 alpha), GL2 alpha (G11 alpha), and Gq alpha expressed in the baculovirus-insect cell system. *J Biol Chem.* 1995;270: 6246–6253.
23. Berstein G, Blank JL, Smrcka AV, et al. Reconstitution of agonist-stimulated phosphatidylinositol 4,5-bisphosphate hydrolysis using purified m1 muscarinic receptor, Gq/11, and phospholipase C-beta 1. *J Biol Chem.* 1992;267:8081–8088.
24. Katz A, Wu D, Simon MI. Subunits beta gamma of heterotrimeric G protein activate beta 2 isoform of phospholipase C. *Nature.* 1992;360: 686–689.

Immunologic and Histopathologic Characterization of an Active Disease Mouse Model for Pemphigus Vulgaris

Manabu Ohyama,* Masayuki Amagai,* Kazuyuki Tsunoda,* Takayuki Ota,*† Shigeo Koyasu,† Jun-ichi Hata,‡ Akihiro Umezawa,‡ and Takeji Nishikawa*

Departments of *Dermatology, †Microbiology and Immunology, and ‡Pathology, Keio University School of Medicine, Shinjuku-ku, Tokyo, Japan

Pemphigus vulgaris is an autoimmune blistering disease of the skin and mucous membranes that is caused by anti-desmoglein 3 IgG autoantibodies. Recently, we generated an active disease mouse model for pemphigus vulgaris by adoptive transfer of splenocytes from immunized desmoglein $3^{-/-}$ mice to $Rag2^{-/-}$ mice. In this study, we performed immunologic and histopathologic studies using this pemphigus vulgaris model in mice and compared the gross and microscopic phenotypes of pemphigus vulgaris model mice and desmoglein $3^{-/-}$ mice. Pemphigus vulgaris model mice showed strong *in vivo* IgG, and weak IgA deposition on keratinocyte cell surfaces in stratified squamous epithelia, and produced circulating anti-desmoglein 3 IgG antibodies without apparent cross-reactivity to desmoglein 1, in enzyme-linked immunosorbent assays. The predominant IgG subclass was IgG1. Pemphigus vulgaris model mice and desmoglein $3^{-/-}$ mice were almost indistinguishable in terms of both gross and microscopic findings. Both types of mice showed suprabasilar acantholysis in the stratified squamous epithelia, including the oral mucous membranes and traumatized skin around the snout or paws; however, some pemphigus vulgaris model mice demonstrated a more severe phenotype than desmoglein $3^{-/-}$ mice. The esophagus and forestomach were affected in some pemphigus vulgaris model mice, but not in desmoglein $3^{-/-}$ mice. Furthermore, eosinophilic spongiosis, which is found in early pemphigus vulgaris lesions in patients, was observed in pemphigus vulgaris model mice but not in desmoglein $3^{-/-}$ mice. Pemphigus vulgaris model mice reflect several of the histopathologic and immunologic features seen in pemphigus vulgaris patients, and provide a valuable tool to investigate the pathophysiologic mechanisms of pemphigus vulgaris. *Key words: autoimmunity/eosinophilic spongiosis/experimental model/knockout mouse/pemphigus. J Invest Dermatol 118:199–204, 2002*

Pemphigus vulgaris (PV) is an autoimmune blistering disease of the skin and mucous membranes that is characterized clinically by flaccid blisters and erosions, and histopathologically by the loss of keratinocyte cell–cell adhesion, resulting in "acantholysis" (Stanley, 1998). The autoimmune target of PV has been identified as desmoglein 3 (Dsg3), a transmembrane desmosomal component that belongs to the cadherin supergene family (Amagai *et al*, 1991, 1994). Accumulated evidence indicates a pathogenic role for anti-Dsg3 IgG autoantibodies in the blister formation that is characteristic of PV (Schiltz and Michel, 1976; Anhalt *et al*, 1982; Hashimoto *et al*, 1983; Merlob *et al*, 1986; Amagai *et al*, 1992; Stanley, 1993; Amagai, 1995). Several attempts have been made to develop animal models to help clarify the pathophysiologic mechanism of PV (Anhalt *et al*, 1982; Juhasz *et al*, 1993; Fan *et al*, 1999).

A passive transfer model using neonatal mice was developed (Anhalt *et al*, 1982). In this model, highly concentrated IgG from the sera of PV patients was injected into neonatal mice and 8–24 h later the mice developed blisters and erosions with the typical pemphigus histology. Subsequently, it was demonstrated that the Fab fragments of IgG purified from PV patients induce similar blistering in neonatal mice (Rock *et al*, 1990; Mascaró *et al*, 1997). Thus, this model provides solid evidence that IgG from patients' sera plays a pathogenic role in inducing blistering, without the involvement of cellular immune responses or complement. This model is still widely used to study the pathogenic role of IgG; however, it reflects only the acute phase (within 24 h) of blister formation. In addition, the blisters are induced in neonatal mice, but not in adult mice. Therefore, the phenotypes of adult mice with PV could not be explored.

In 1997, Dsg3-knockout mice were produced by genetic disruption of *DSG3* (Koch *et al*, 1997). $Dsg3^{-/-}$ mice showed extensive erosions in the oral mucous membranes with suprabasilar acantholysis, which resulted in weight loss due to insufficient food intake. Erosive lesions were also found in traumatized skin. These findings clearly demonstrated the important *in vivo* role of Dsg3 in the cell–cell adhesion of keratinocytes. In addition, $Dsg3^{-/-}$ mice demonstrated telogen hair loss, providing the first cutaneous manifestation of Dsg3 dysfunction in adult mice (Koch *et al*, 1998). These findings also suggested that anti-Dsg3 autoantibodies directly interfered with the adhesive function of Dsg3 to cause blisters; however, no immunologic components were involved in determining the phenotype of the $Dsg3^{-/-}$ mice.

Manuscript received July 28, 2001; revised October 10, 2001; accepted for publication October 18, 2001.

Reprint requests to: Dr. Manabu Ohyama, Department of Dermatology, Keio University School of Medicine, 35 Shinanomachi, Shinjuku-ku, Tokyo 160-8582, Japan. Email: maboym@sc.itc.keio.ac.jp

Abbreviations: PV, pemphigus vulgaris; Dsg, desmoglein; rDsg, recombinant Dsg.

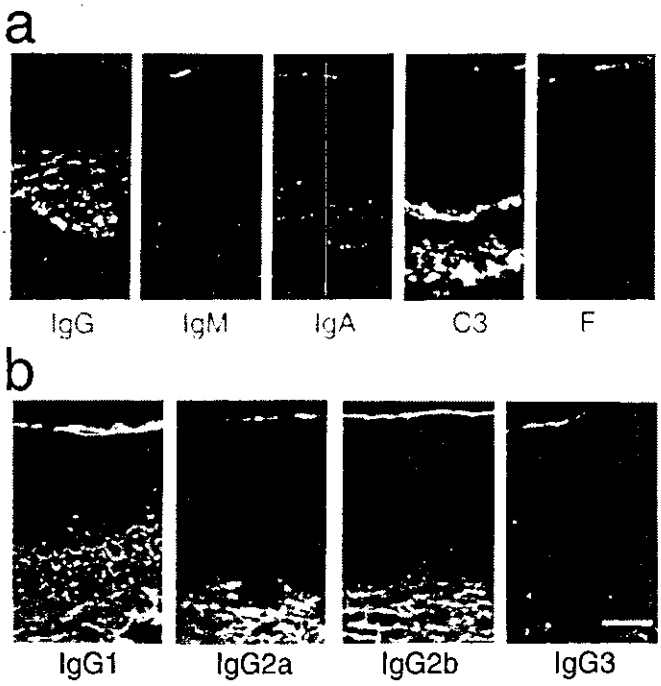

Figure 1. Predominant IgG1 deposition on keratinocyte surfaces in PV model mice *in vivo*. (*a*) Strong IgG and very weak IgA deposition was observed on the surfaces of keratinocytes of the palate of PV model mice. F, fibrinogen. (*b*) IgG1 was predominantly observed in the intercellular space. IgG2a and IgG2b were weakly detected and no apparent IgG3 deposition was observed. *Scale bar*: 50 μm.

An active disease mouse model for PV was generated by a novel approach, using $Dsg3^{-/-}$ mice that could not be tolerized against Dsg3 (Amagai *et al*, 2000). After the $Dsg3^{-/-}$ mice were immunized with mouse recombinant Dsg3 (rDsg3), splenocytes from the immunized mice were transferred into $Rag2^{-/-}$ mice that expressed Dsg3. T and B cells from $Dsg3^{-/-}$ mice were stimulated with endogenous Dsg3 in the recipient mice, and anti-Dsg3 IgG was stably produced for over 6 mo. The anti-Dsg3 IgG bound to Dsg3 *in vivo* and caused blisters and erosions in the oral mucous membranes as well as in traumatized skin with suprabasilar acantholysis. The recipient mice also showed telogen hair loss.

In this study, we characterized PV model mice both immunologically and histopathologically and compared the gross and microscopic phenotypes of PV model and $Dsg3^{-/-}$ mice. We determined the specificity and the IgG subclass of antibodies raised in the PV model mice. We performed detailed histopathologic investigations of PV model and $Dsg3^{-/-}$ mice and compared the distribution of affected sites and the severity of phenotype. Moreover, we determined whether PV model mice showed eosinophilic spongiosis, which is a characteristic histologic finding in the early lesions of PV patients (Emmerson and Wilson Jones, 1968; Knight *et al*, 1976; Pearson *et al*, 1980).

MATERIALS AND METHODS

Mice $Dsg3^{-/-}$ mice were obtained by mating male $Dsg3^{-/-}$ and female $Dsg3^{+/-}$ mice (The Jackson Laboratory, Bar Harbor, ME). These mice have a mixed genetic background of 129/SV ($H\text{-}2^b$) and C57BL/6J ($H\text{-}2^b$). $Rag2^{-/-}$ mice that had been backcrossed to B6.SJL-*Ptprc*^{a} mice for 10 generations (Schulz *et al*, 1996) were purchased from Taconic Farms (Germantown, NY).

PV model mice PV model mice were prepared as previously reported (Amagai *et al*, 2000). Briefly, $Dsg3^{-/-}$ mice were primed once with 10 μg of purified mouse rDsg3 in complete Freund's adjuvant, then immunized twice with incomplete Freund's adjuvant and twice without adjuvant. Antibody production was examined regularly by enzyme-linked immunosorbent assay (ELISA) using mouse rDsg3. Splenocytes were isolated from $Dsg3^{-/-}$ mice after immunization and injected intravenously into $Rag2^{-/-}$ mice.

Direct immunofluorescence Five PV model mice were killed and biopsy specimens were taken from the snout, palate, esophagus, and forestomach, and embedded in OCT compound (Sakura Finetechnical, Tokyo, Japan) for cryostat sectioning. For standard direct immunofluorescence studies, each section was incubated with a 100-fold dilution of fluorescein isothiocyanate-rabbit anti-mouse IgG antibody (Zymed Laboratories, San Francisco, CA), fluorescein isothiocyanate-goat anti-mouse IgM, IgA, C3 (Cappel Product, Aurora, OH) and fibrinogen IgG fractions (Nordic Immunological Laboratories, Tilburg, the Netherlands). For subclass determinations, the sections were first incubated with a 50-fold dilution of rat anti-mouse IgG1, IgG2a, IgG2b, and IgG3 monoclonal antibodies (PharMingen, San Diego, CA) and, after washing in phosphate-buffered saline, stained secondarily with a 1000-fold dilution of Alexa Fluor 488-goat anti-rat IgG antibody (Molecular Probes, Eugene, OR). All of the sections were examined using a fluorescence microscope (Eclipse E800, Nikon, Tokyo, Japan).

ELISA ELISA using recombinant mouse Dsg1 and Dsg3 were performed, essentially as previously described for human Dsg1 and Dsg3 ELISA (Ishii *et al*, 1997; Amagai *et al*, 1999). First, the ELISA plate was coated with 2.5 μg per ml of mouse rDsg1 and rDsg3 expressing the entire extracellular domain (Amagai *et al*, 2000). For anti-Dsg3 IgG, IgA, IgM, and anti-Dsg1 IgG ELISA, 5000-fold dilutions of PV mouse serum were incubated for 1 h on individual ELISA plates. After washing, the plates were incubated with 5000-fold dilutions of peroxidase-labeled goat anti-mouse IgG, IgA and IgM polyclonal antibodies (Zymed Laboratories) for 1 h. The plates were then washed, and color development was performed using a solution containing equal amounts of tetramethylbenzidine and hydrogen peroxide (Medical Biological Laboratories, Nagano, Japan) for 30 min; the reaction was stopped by adding 100 μl of 4 M H_2SO_4. The optical density (OD) of each sample was measured at 450 nm in a microplate reader (Bio-Rad Laboratories, Hercules, CA).

For the IgG subclass ELISA, 1000-fold dilutions of sera from PV model mice were incubated for 45 min in plates that had been coated with mouse rDsg3. After washing, the plates were incubated with a 1000-fold dilution of rat anti-mouse IgG1, IgG2a, IgG2b, and IgG3 monoclonal antibodies (PharMingen, San Diego, CA) for 45 min, and washed once more. All of the plates were incubated with a 2500-fold dilution of peroxidase-labeled goat anti-rat IgG polyclonal antibody for 45 min, washed, developed and analyzed as described above. Thirty-one PV model mouse sera and 10 normal mouse sera were analyzed for subclass with anti-Dsg3 IgG, IgA, and IgM, or anti-Dsg1 IgG. For the IgG subclass ELISA, 20 PV model mouse sera and 10 normal control sera were analyzed for each individual subclass.

We calculated the mean and SD for each subclass ELISA using the OD values of normal controls. Based on the value obtained from the formula: mean + 3 SD, we set cut-off values of 0.10 for anti-Dsg1 IgG ELISA, 0.027 for anti-Dsg3 IgG, IgA, and IgM ELISA, and 0.062 for IgG subclass ELISA.

Histopathologic analysis We examined 15 PV model mice and 15 $Dsg3^{-/-}$ mice and a normal C57BL/6J mouse. The entire animal skin was cut into small strips of about 1.5 mm by 20 mm for extensive histopathologic analysis. These strips were arranged in continuous order in plastic cassettes in order to preserve the original orientation. The head, limbs, and tail were decalcified and cut into serial sections at 1.5 mm spacings. The esophagus, forestomach, stomach, small and large intestine, lung, liver, heart, and kidney were taken separately and serial sections were prepared. All these sections were stained with hematoxylin and eosin and examined by light microscopy. The distribution of suprabasilar acantholysis; erosion, and spongiosis was noted. A lesion was defined as an affected site in cases where a microscopic lesion with suprabasilar acantholysis was spatially separated from other lesions by normal epidermis. The number of affected sites per individual mouse was counted for each mouse group.

Eosinophil staining To assess the presence of eosinophilic spongiosis, 52 sites in 19 sections from nine PV model mice and 40 sites in 16 sections from seven $Dsg3^{-/-}$ mice, all of which had apparent spongiosis, were selected and stained with Chromotrope 2R (Lendrum, 1944) and hematoxylin. In this study, eosinophilic spongiosis was diagnosed when

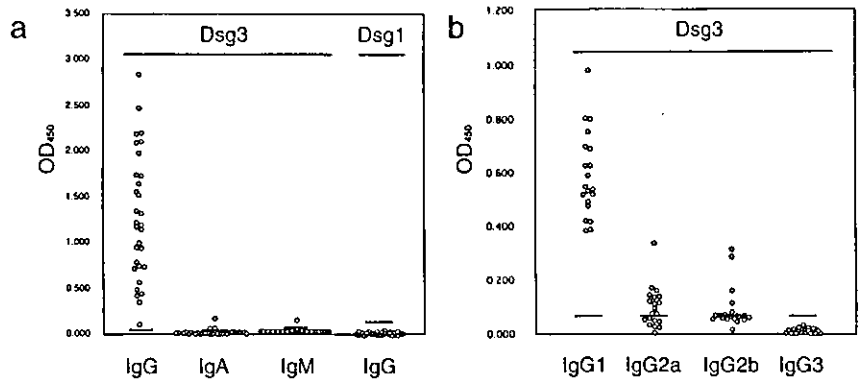

Figure 2. Circulating IgG1 against mouse Dsg3 predominates in sera obtained from PV model mice. (*a*) All 31 PV model mice sera were positive for anti-Dsg3 IgG, whereas all were negative for anti-Dsg1 IgG. Three and one sera were slightly positive for anti-Dsg3 IgA and IgM, respectively. (*b*) All 20 PV model mice sera showed positive in IgG1 ELISA, whereas 12 sera were positive for IgG2a and IgG2b. No sera were positive for IgG3. Bars indicate the cut-off values determined for individual ELISA.

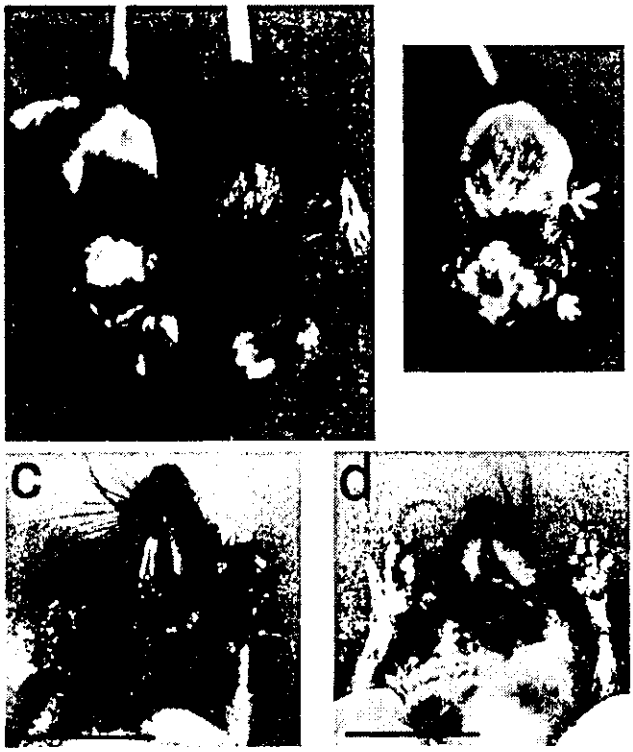

Figure 3. Gross phenotypes of PV model and Dsg3$^{-/-}$ mice. Compared with the wild-type B6 mouse (*a*, right), PV model mice (*a*, left) showed patchy telogen hair loss and weight loss. Dsg3$^{-/-}$ mice also showed patchy telogen hair loss and weight loss (*b*), similar in extent to the PV model mice. Some PV model mice showed crust-covered severe erosions on the paws, and elongated front teeth (*c*), whereas Dsg3$^{-/-}$ mice rarely showed these changes (*d*). *Scale bar:* 2 cm.

more than three exocytic eosinophils were observed in the intercellular space under × 400 magnification.

RESULTS

Predominant IgG1 subclass for anti-Dsg3-specific IgG autoantibodies in the PV model mouse A direct immunofluorescence study was performed to delineate both the class and subclass of predominant immunoglobulins that were deposited in the intercellular space *in vivo*. Immunostaining of the PV model mouse palate showed strong IgG deposition on keratinocyte cell surfaces (**Fig 1*a***). Although weak deposition of IgA was also detected in the intercellular space, the staining pattern tended to be granular. Broad C3 deposition was observed around the basement membrane zone, probably due to local inflammation. No depositions of IgM or fibrinogen were observed. IgG subclass staining revealed that IgG1 was predominant, with distinct linear deposition patterns on keratinocyte surfaces (**Fig 1*b***). Weak deposition of IgG2a and IgG2b was also observed in the intercellular space, whereas no IgG3 deposition was detected.

ELISA using mouse rDsg1 and rDsg3 were used to determine the immunoglobulin class of circulating autoantibodies. All 31 PV model mice sera were positive for anti-Dsg3 IgG, but negative for anti-Dsg1 IgG (**Fig 2*a***). Most of the sera were negative for anti-Dsg3 IgA or anti-Dsg3 IgM, although three of 31 and one of 31 sera slightly exceeded the cut-off values for anti-Dsg3 IgA and anti-Dsg3 IgM, respectively.

An IgG subclass ELISA was performed with mouse rDsg3 to investigate further the subclasses of circulating anti-Dsg3 IgG in PV model mice (**Fig 2*b***). All 20 sera were positive for IgG1, with a mean OD value of 0.59, whereas 12 of 20 sera were positive for IgG2a and Ig2b with lower mean OD values of 0.097 and 0.090, respectively. No sera were positive for IgG3 (mean OD of 0.009).

Some PV model mice have a more severe phenotype than Dsg3$^{-/-}$ mice PV model mice weighed less and had patchy hair loss compared with normal mice (Amagai *et al*, 2000). The weight loss was probably because oral erosions, arising from the presence of anti-Dsg3 IgG, discouraged food intake. The patchy baldness was due to telogen hair loss (Koch *et al*, 1997; Amagai *et al*, 2000). Encrusted erosions on the traumatized skin around snouts, eyes, ears, paws, and tails were also observed in PV model mice (**Fig 3*a***). These characteristics were also observed in Dsg3$^{-/-}$ mice (**Fig 3*b***); however, some PV model mice showed heavily encrusted erosions on the paws and elongated front teeth (**Fig 3*c***). It was likely that these mice were unable to gnaw solid food because of painful oral erosions and this resulted in tooth elongation. Severe defects such as these were rarely observed among Dsg3$^{-/-}$ mice (**Fig 3*d***).

Suprabasilar acantholysis is observed in similar distribution in both mice, except in esophagus and forestomach The distribution of suprabasilar acantholysis, a typical histologic finding of PV, was intensively examined in serial sections of the skin and mucous membranes of PV model and Dsg3$^{-/-}$ mice (n = 15 for each mouse group) (**Table I**). In general, the distribution was similar in PV model and Dsg3$^{-/-}$ mice. Both types of mouse had skin lesions on the snout, eyelid, ear, trunk, paw, and tail, i.e., areas that are normally traumatized by scratching or constant physical pressure (**Fig 4*a–f***). Both PV model and Dsg3$^{-/-}$ mice showed lesions in the squamous mucosae of the tongue, buccal mucosa, palate, and larynx (**Fig 4*g*, *h***); however, some PV model mice also

Table I. Distribution of affected tissues with suprabasilar acantholysis in PV model mice and Dsg3$^{-/-}$ mice in histology[a]

ìite	PV model mouse (n = 15)	Dsg3$^{-/-}$ mouse (n = 15)
ìkin		
snout	12	9
eyelid	7	7
ear	14	11
trunk	5	2
paw	12	7
tail	8	2
ìquamous mucosa		
tongue	7	5
buccal mucosa	2	2
palate	10	4
larynx	6	4
esophagus	3	0
forestomach	1	0
.ung	0	0
.iver	0	0
ìtomach	0	0
ntestine	0	0
Ìidney	0	0

[a]Numbers of mice with involvement at the designated tissue were indicated.

ıad lesions in the esophagus and squamocolumnar junction of the ɔrestomach (**Fig 4*i, j***). Lesions in these areas have not been seen in)sg3$^{-/-}$ mice, as described in the original report (Koch *et al*, 1997).)ense inflammatory infiltrations of lymphocytes and neutrophils, ırobably as a result of secondary inflammation after barrier lisruption, were noted in both PV model and Dsg3$^{-/-}$ mice **Fig 4*a–d***). Early lesions were not accompanied by inflammatory ell infiltrates. No pathologic abnormalities were observed in the ungs, hearts, kidneys, livers, or intestines of any mice (**Table I**).

'V model mice show a broader variety of lesions than)sg3$^{-/-}$ mice To compare the extent of lesion formation in PV nodel and Dsg3$^{-/-}$ mice in a quantitative fashion, the number of ites with suprabasilar acantholysis in histology was counted for ach of 15 PV model and Dsg3$^{-/-}$ mice (**Fig 5**). In this assay, hair ollicle involvement was excluded because it was hair-cycle lependent. The Dsg3$^{-/-}$ mouse group showed one to six affected ites per mouse, with a mean value of 3.9 ± 1.8. In contrast, the 'V model mouse group showed three to 11 affected sites per nouse, with a mean value of 6.6 ± 3.1. The PV model mice had nore affected sites than the Dsg3$^{-/-}$ mice ($p = 0.02$, Mann–Whitney analysis). Among the mice tested, seven PV model mice ıad more lesions than any of the Dsg3$^{-/-}$ mice. Therefore, PV nodel mice exhibited broader variation in the number of lesions han Dsg3$^{-/-}$ mice and some PV model mice had more severe ɛsions.

ɛosinophilic spongiosis in PV model mice PV patients lisplay spongiosis accompanied by eosinophilic cell infiltrations in arly erythematous lesions. This phenomenon is known as 'eosinophilic spongiosis" (Emmerson and Wilson Jones, 1968; Knight *et al*, 1976; Pearson *et al*, 1980). To evaluate whether the ıuman histologic changes were reproduced in the PV model nouse, we stained spongiotic sections of both PV model and)sg3$^{-/-}$ mice with Chromotrope 2R. We defined eosinophilic pongiosis as spongiosis with more than three exocytic eosinophils ı the intercellular space. On this basis, eosinophilic spongiosis was ɔbserved at 12 of 52 sites with spongiotic change in 19 sections ɔm PV model mice (n = 9) (**Fig 6*a***). In contrast, no eosinophilic pongiosis was found at 40 spongiotic sites in 16 sections from)sg3$^{-/-}$ mice (n = 7) (**Fig 6*b***), although occasional dermal osinophil infiltrations were observed in a few sections.

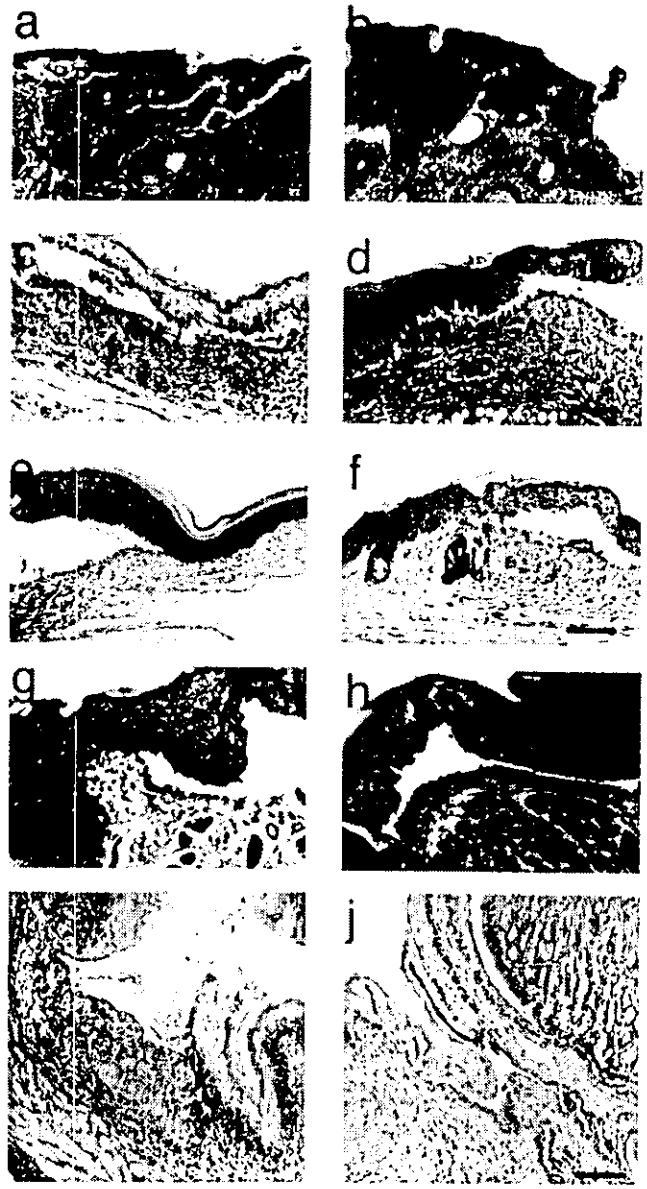

Figure 4. Histopathologic comparisons of PV model and Dsg3$^{-/-}$ mice. Histopathologic findings in PV model mice (*a, c, e, g, i, j*) and Dsg3$^{-/-}$ mice (*b, d, f, h*). Suprabasilar acantholysis was observed with similar distribution on the traumatized skin (*a, b,* snout; *c, d,* ear; *e, f,* paw) and mucous membranes (*g, h*: hard palate); however, involvement of the esophagus and forestomach was observed only in PV model mice (*i, j*). Mucosal epithelia were detached from the lamina propria mucosae with inflammatory cell infiltrations (*i,* esophagus). Acantholysis was observed around the squamocolumnar junction (*j,* forestomach). *Scale bar:* 50 μm (hematoxylin and eosin staining).

DISCUSSION

In this study, we immunologically and histopathologically characterized novel PV model mice and compared the gross and microscopic phenotypes of PV model and Dsg3$^{-/-}$ mice. The predominant subclass *in vivo* of both bound and circulating anti-Dsg3 antibodies was IgG1. In addition to IgG1, weak anti-Dsg3 IgG2a and IgG2b were also detected, both *in vivo* and *in vitro*. Although there were weak granular deposits of IgA in the mouse skin, the significance of this finding is unclear, as we did not detect any significant circulating IgA against Dsg3 by ELISA. Thus, the predominant, pathogenic anti-Dsg3 autoantibodies produced in the PV model mouse were of the IgG1 type. IgG4 is predominant over IgG in human PV (David *et al*, 1989; Yamada *et al*, 1989; Shirakata

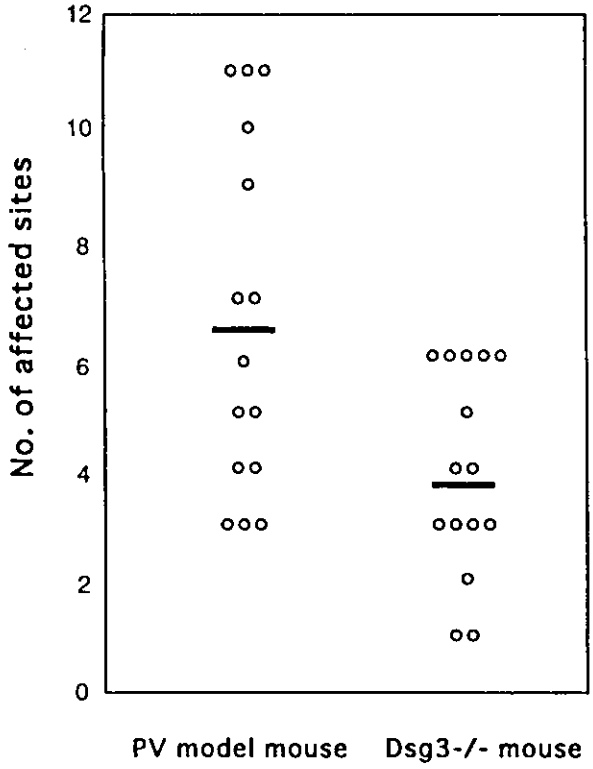

Figure 5. Affected sites in PV model and Dsg3$^{-/-}$ mice. The number of affected sites per mouse was counted for PV model and Dsg3$^{-/-}$ mice. Some PV model mice were more severely affected and PV model mice showed broader variations in the extent of microscopic lesions than Dsg3$^{-/-}$ mice. Bars indicate the mean values for each group.

et al, 1990; Dmochowski *et al*, 1992; Futei *et al*, 2001). Interestingly, although there is no distinct correlation between the human and mouse IgG subclasses, human IgG4 resembles mouse IgG1 in its inability to fix complement (Brüggemann *et al*, 1987; Dangl *et al*, 1988). We are aware that the PV model does not mimic the onset of human PV, because production of the pathogenic anti-Dsg3 IgG is initiated by the adoptive transfer of splenocytes from Dsg3$^{-/-}$ mice to Dsg3$^{+/+}$ mice. The importance of the noncomplement-fixing IgG subclasses, however, brings the murine PV model closer to human PV in terms of events that occur after antibody binding to Dsg3.

PV model mice were almost indistinguishable from Dsg3$^{-/-}$ mice in gross as well as microscopic appearance. Both types of mouse showed cell–cell adhesion loss, i.e., suprabasilar acantholysis, in the stratified squamous epithelia, including the oral mucous membranes and the skin where scratching or constant physical pressure occurred (**Table I, Figs 3** and **4**); however, some PV model mice demonstrated more severe phenotypes than the Dsg3$^{-/-}$ mice. These PV model mice showed features such as heavily encrusted erosions on the paws and elongated front teeth, which were rarely found in Dsg3$^{-/-}$ mice. The involvement of the esophagus and forestomach was found in some PV model mice, but not in Dsg3$^{-/-}$ mice. To evaluate these subtle phenotypic differences in a quantitative fashion, the number of affected sites with suprabasilar acantholysis was counted under microscopy. Among the mice tested, about 50% of the PV model mice (seven of 15) had more lesions than any of the Dsg3$^{-/-}$ mice, indicating that some PV model mice had more severe microscopic defects than the Dsg3$^{-/-}$ mice. On the other hand, approximately 15–20% of the mice that underwent adoptive transfer of immunized Dsg3$^{-/-}$ splenocytes did not develop the PV phenotype, in spite of circulating anti-Dsg3 IgG, probably due to insufficient amounts of anti-Dsg3 IgG (Amagai *et al*, 2000). Therefore, PV model mice show greater variety in the extent of lesions than Dsg3$^{-/-}$ mice.

Figure 6. Eosinophilic spongiosis in PV model mice. Eosinophilic cell infiltrations in the intercellular space of the epidermis were found in some spongiotic sites of PV model mice (*a*), but not in those of Dsg3$^{-/-}$ mice (*b*). *Arrows* indicate eosinophils. *Scale bar*: 50 μm (Chromotrope 2R and hematoxylin staining).

Why do PV model mice and Dsg3$^{-/-}$ mice show this subtle phenotypic difference? Is this variation caused by differences in their genetic backgrounds? In the adoptive transfer experiment, we used Rag2$^{-/-}$ recipient mice that were backcrossed to B6.SJL-*Ptprc*^{a} mice for 10 generations (Schulz *et al*, 1996). The Dsg3$^{-/-}$ mice had a mixed genetic background of 129/SV(H-2^{b}) and C57BL/6J(H-2^{b}) (Koch *et al*, 1997). If genetic background plays a part, it should apply to both PV model and Dsg3$^{-/-}$ mice. The major difference between PV model and Dsg3$^{-/-}$ mice is that Dsg3 function is blocked by IgG antibodies in PV model mice, whereas Dsg3 is genetically depleted in Dsg3$^{-/-}$ mice. Therefore, the overall similarities between PV model mice and Dsg3$^{-/-}$ mice suggest that acantholysis is caused in the PV model mice by direct interference from anti-Dsg3 IgG antibodies. The differences between PV model and Dsg3$^{-/-}$ mice, however, suggest that, in addition to antibody–antigen interactions, another factor may play a part in the clinical appearance of PV. In PV model mice, as in patients with PV, anti-Dsg3 IgG binds to Dsg3 on keratinocyte cell surfaces and remains associated for weeks, even in skin of normal appearance. Therefore, it is possible that long-lasting antibody–antigen interactions on keratinocytes might cause secondary inflammatory reactions via signal transduction or cytokine release, thus leading to phenotypic modifications. This type of reaction cannot be studied with the previous passive-transfer model using neonatal mice, because that model represents only the acute phase of blister formation.

One of the characteristic histologic features of pemphigus is eosinophilic spongiosis, a term coined by Emmerson and Wilson Jones (1968). Eosinophilic spongiosis was regarded initially as one of the specific traits of pemphigus (Knight *et al*, 1976; Pearson *et al*, 1980), but now it is accepted that this histologic reaction is not only observed in pemphigus (and PV) but also in other autoimmune blistering diseases, such as bullous pemphigoid (Crotty *et al*, 1983; Nishioka *et al*, 1984; Machado-Pinto *et al*, 1996). Although this histologic finding is well described in the literature, the pathophysiologic significance of eosinophilic spongiosis has remained elusive. Recently, Th2 cytokines, such as interleukin-5, and chemokines, such as RANTES or eotaxin, have been implicated in cutaneous eosinophil infiltration (Ying *et al*, 1995; Schröder *et al*, 1996; Moine *et al*, 1999; Yawalkar *et al*, 1999), and keratinocytes are able to produce such factors (Li *et al*, 1996; Wakugawa *et al*, 2000). In addition, patients with bullous pemphigoid may have elevated eosinophil chemoattractants in their sera or bullous fluids, which may result in eosinophilia (D'Auria *et al*, 1998; Rico *et al*, 1999; Shrikhande *et al*, 2000;

Wakugawa *et al*, 2000); however, no data supporting the involvement of interleukin-5 or RANTES in eosinophilic infiltrations in PV have been reported to date (Bornscheuer *et al*, 1999; Rico *et al*, 1999). Eosinophilic spongiosis was demonstrated in PV model mice with Chromotrope 2R staining, although no apparent eosinophilic infiltration was observed in Dsg3$^{-/-}$ mice. Therefore, the PV model mouse provides a valuable tool to investigate unknown molecular mechanisms in the formation of eosinophilic spongiosis and their role in the pathogenesis of PV.

We thank Mr Satoru Kusakari and all of the technical assistants at the Department of Pathology, Keio University School of Medicine for preparing pathologic slides, and Ms. Minae Suzuki for immunofluorescence staining. This work was supported by Health Science Research Grants for Research on Specific Disease from the Ministry of Health, Labor and Welfare, and Grants-in-Aid for Scientific Research from the Ministry of Education, Culture, Science and Technology of Japan.

REFERENCES

Amagai M: Adhesion molecules I: keratinocyte–keratinocyte interactions, cadherins and pemphigus. *J Invest Dermatol* 104:146–152, 1995

Amagai M, Klaus-Kovtun V, Stanley JR: Autoantibodies against a novel epithelial cadherin in pemphigus vulgaris, a disease of cell adhesion. *Cell* 67:869–877, 1991

Amagai M, Karpati S, Prussick R, Klaus-Kovtun V, Stanley JR: Autoantibodies against the amino-terminal cadherin-like binding domain of pemphigus vulgaris antigen are pathogenic. *J Clin Invest* 90:919–926, 1992

Amagai M, Hashimoto T, Shimizu N, Nishikawa T: Absorption of pathogenic autoantibodies by the extracellular domain of pemphigus vulgaris antigen (Dsg3) produced by baculovirus. *J Clin Invest* 94:59–67, 1994

Amagai M, Komai A, Hashimoto T, *et al*: Usefulness of enzyme-linked immunosorbent assay (ELISA) using recombinant desmogleins 1 and 3 for serodiagnosis of pemphigus. *Br J Dermatol* 140:351–357, 1999

Amagai M, Tsunoda K, Suzuki H, Nishifuji K, Koyasu S, Nishikawa T: Use of autoantigen-knockout mice in developing an active autoimmune disease model for pemphigus. *J Clin Invest* 105:625–631, 2000

Anhalt GJ, Labib RS, Voorhees JJ, Beals TF, Diaz LA: Induction of pemphigus in neonatal mice by passive transfer of IgG from patients with the disease. *N Engl J Med* 306:1189–1196, 1982

Bornscheuer E, Zillikens D, Schröder JM, Stucherling M: Lack of expression of interleukin 8 and RANTES in autoimmune bullous skin disease. *Dermatology* 198:118–121, 1999

Brüggemann M, Williams GT, Bindon CI, *et al*: Comparison of the effector functions of human immunoglobulins using a matched set of chimeric antibodies. *J Exp Med* 166:1351–1361, 1987

Crotty C, Pittelkow M, Muller SA: Eosinophilic spongiosis. A clinicopathologic review of seventy-one cases. *J Am Acad Dermatol* 8:337–343, 1983

D'Auria L, Pietravalle M, Mastroianni A, *et al*: IL-5 levels in the serum and blister fluid of patients with bullous pemphigoid: correlations with eosinophil cationic protein, RANTES, IgE, and disease severity. *Arch Dermatol Res* 290:25–27, 1998

Dangl JL, Wensel TG, Morrison SL, Stryer L, Herzenberg LA, Oi VT: Segmental flexibility and complement fixation of genetically engineered chimeric human, rabbit and mouse antibodies. *EMBO J* 7:1989–1994, 1988

David M, Katzenelson V, Hazaz B, Ben CA, Sandbank M: Determination of IgG subclasses in patients with pemphigus with active disease and in remission. *Arch Dermatol* 125:787–790, 1989

Dmochowski M, Hashimoto T, Nishikawa T: The analysis of IgG subclasses of anti-intercellular antibodies in pemphigus by an immunoblot technique. *Arch Dermatol Res* 284:309–311, 1992

Emmerson RW, Wilson Jones E: Eosinophilic spongiosis in pemphigus. *Arch Dermatol* 97:252–257, 1968

Fan J, Memar O, McCormick DJ, Prabhakar BS: BALB/c mice produced blister-causing antibodies upon immunization with a recombinant human desmoglein 3. *J Immunol* 163:6228–6235, 1999

Futei Y, Amagai M, Ishii K, Kuroda-Kinoshita K, Ohya K, Nishikawa T: Predominant IgG4 subclass in autoantibodies of pemphigus vulgaris and foliaceus. *J Dermatol Sci* 26:55–61, 2001

Hashimoto K, Shafran KM, Webber PS, Lazarus GS, Singer KH: Anti-cell surface pemphigus autoantibody stimulates plasminogen activator activity of human epidermal cells. *J Exp Med* 157:259–272, 1983

Ishii K, Amagai M, Hall RP, *et al*: Characterization of autoantibodies in pemphigus using antigen-specific ELISA with baculovirus expressed recombinant desmoglein. *J Immunol* 159:2010–2017, 1997

Juhasz I, Lazarus GS, Murphy GF, Shih IM, Herlyn M: Development of pemphigus vulgaris-like lesions in severe combined immunodeficiency disease mice reconstituted with lymphocytes from patients. *J Clin Invest* 92:2401–2407, 1993

Knight AG, Black MM, Delaney TJ: Eosinophilic spongiosis. A clinical histological and immunofluorescent correlation. *Clin Exp Dermatol* 1:141–153, 1976

Koch PJ, Mahoney MG, Ishikawa H, *et al*: Targeted disruption of the pemphigus vulgaris antigen (desmoglein 3) gene in mice causes loss of keratinocyte cell adhesion with a phenotype similar to pemphigus vulgaris. *J Cell Biol* 137:1091–1102, 1997

Koch PJ, Mahoney MG, Cotsarelis G, Rothenberger K, Lavker RM, Stanley JR: Desmoglein 3 anchors telogen hair in the follicle. *J Cell Sci* 111:2529–2537, 1998

Lendrum AG: The staining of eosinophil polymorphs and enterochromaffin cells in histological sections. *J Pathol Bacteriol* 56:441, 1944

Li J, Ireland GW, Farthing PM, Thornhill MH: Epidermal and oral keratinocytes are induced to produce RANTES and IL-8 by cytokine stimulation. *J Invest Dermatol* 106:661–666, 1996

Machado-Pinto J, McCalmont TH, Goltz LE: Eosinophilic and neutrophilic spongiosis: Clues to the diagnosis of immunobullous diseases and other inflammatory disorders. *Semin Cutan Med Surg* 15:308–316, 1996

Mascaró JM, España A, Liu Z, Ding X, Swartz SJ, Fairley JA, Diaz LA: Mechanism of acantholysis in pemphigus vulgaris: Role of IgG Valence. *Clin Immunol Immunopathol* 85:90–96, 1997

Merlob P, Metzker A, Hazaz B, Rogovin H, Reisner SH: Neonatal pemphigus vulgaris. *Pediatrics* 78:1102–1105, 1986

Moine AL, Surquin M, Demoor FX, *et al*: IL-5 mediates eosinophilic rejection of MHC class II-disparate skin allografts in mice. *J Immunol* 163:3778–3784, 1999

Nishioka K, Hashimoto K, Katayama I, Sarashi C, Kubo T, Sano S: Eosinophilic spongiosis in bullous pemphigoid. *Arch Dermatol* 120:1166–1168, 1984

Pearson RW, O'Donoghue M, Kaplan SJ: Pemphigus vegetans. its relationship to eosinophilic spongiosis and favorable response to dapsone. *Arch Dermatol* 116:65–68, 1980

Rico MJ, Benning C, Weingart ES, Streilein RD, Hall RP: Characterization of skin cytokines in bullous pemphigoid and pemphigus vulgaris. *Br J Dermatol* 140:1079–1086, 1999

Rock B, Labib RS, Diaz LA: Monovalent Fab′ immunoglobulin fragments from endemic pemphigus foliaceus autoantibodies reproduce the human disease in neonatal Balb/c mice. *J Clin Invest* 85:296–299, 1990

Schiltz JR, Michel B: Production of epidermal acantholysis in normal human skin in vitro by the IgG fraction from pemphigus serum. *J Invest Dermatol* 67:254–260, 1976

Schröder JM, Noso N, Stuchering M, Christophers E: Role of eosinophil-chemotactic C-C chemokines in cutaneous inflammation. *J Leukoc Biol* 59:1–5, 1996

Schulz RJ, Parkes A, Mizoguchi E, Bhan AK, Koyasu S: Development of $CD4^-CD8^-$ $\alpha\beta TCR^+NK1.1^+$ T lymphocytes: thymic selection by self antigen. *J Immunol* 157:4379–4389, 1996

Shirakata Y, Shiraishi S, Sayama K, Miki Y: Subclass characteristics of IgG autoantibodies in bullous pemphigoid and pemphigus. *J Dermatol* 17:661–666, 1990

Shrikhande M, Hunziker T, Braathen LR, Pichler WJ, Dahinden CA: Increased coexpression of eotaxin and interleukin 5 in bullous pemphigoid. *Acta Derm Venereol* 80:277–280, 2000

Stanley JR: Cell adhesion molecules as targets of autoantibodies in pemphigus and pemphigoid, bullous diseases due to defective epidermal cell adhesion. *Adv Immunol* 53:291–325, 1993

Stanley JR: Pemphigus. In: Freedberg IM, Eisen AZ, Wolff K, Austen KF, Goldsmith LA, Katz SI, Fitzpatrick TB (eds). *Dermatology in General Medicine*. New York: McGraw-Hill, 1998; pp 654–666

Wakugawa M, Nakamura K, Hino H, *et al*: Elevated levels of eotaxin and interleukin-5 in blister fluid of bullous pemphigoid: correlation with tissue eosinophilia. *Br J Dermatol* 143:112–116, 2000

Yamada H, Hashimoto T, Nishikawa T: IgG subclasses of intercellular and basement membrane zone antibodies: the relationship to the capability of complement fixation. *J Invest Dermatol* 92:585–587, 1989

Yawalkar N, Uguccioni M, Schärer J, *et al*: Enhanced expression of eotaxin and CCR3 in atopic dermatitis. *J Invest Dermatol* 113:43–48, 1999

Ying BS, Taborda-Barata L, Meng Q, Humbert M, Kay AB: The kinetics of allergen-induced transcription of messenger RNA for monocyte chemotactic protein-3 and RANTES in the skin of human atopic subjects: Relationship to eosinophil, T cell, and macrophage recruitment. *J Exp Med* 181:2153–2159, 1995

Differentiation (2001) 68:235–244

ORIGINAL ARTICLE

Jun Kohyama · Hitoshi Abe · Takuya Shimazaki
Amane Koizumi · Kinichi Nakashima · Satoshi Gojo
Tetsuya Taga · Hideyuki Okano · Jun-ichi Hata
Akihiro Umezawa

Brain from bone: Efficient "meta-differentiation" of marrow stroma-derived mature osteoblasts to neurons with Noggin or a demethylating agent

Accepted in revised form: 26 June 2001

Abstract Bone marrow stromal cells are able to differentiate into adipogenic, chondrogenic, myogenic, osteogenic, and cardiomyogenic lineages, all of which are limited to a mesoderm-derived origin. In this study, we showed that neurons, which are of an ectoderm-origin, could be generated from marrow-derived stromal cells by specific inducers, fibronectin/ornithine coating, and neurosphere formation. The neurons generated from marrow stroma formed neurites, expressed neuron-specific markers and genes, and started to respond to depolarizing stimuli as functional mature neurons. Among stromal cells, isolated mature osteoblasts which had strong *in vivo* osteogenic activity could be efficiently converted into functional neurons. This transdifferentiation or meta-differentiation was enhanced by Noggin, an inhibitor of bone morphogenetic proteins, in comparison with 5-azacytidine, a demethylating agent capable of altering the gene expression pattern. Marrow stroma is therefore a potential source of cells for neural cell transplantation.

J. Kohyama[1] · H. Abe[1] · T. Shimazaki[2] · A. Koizumi[2] · H. Okano[2] · J. Hata[1] · A. Umezawa[1] (✉)
Department of Pathology[1] and Physiology[2], Keio University School of Medicine, 35 Shinanomachi, Shinjuku-ku, Tokyo 160-8582, Japan
e-mail: umezawa@1985.jukuin.keio.ac.jp
Tel: +81 3 5363 3764, Fax: +81 3 3353 3290

T. Shimazaki · H. Okano
Division of Neuroanatomy, Osaka University Graduate School of Medicine, 2-2 Yamadaoka, Suita, Osaka 565-0871, Japan

K. Nakashima · T. Taga
Department of Cell Fate Modulation, Institute of Molecular Embryology and Genetics, Kumamoto University 2-2-1, Honjo, Kumamoto 860-0811, Japan

S. Gojo
Department of Cardiac Surgery, Saitama Medical Center, Kawagoe, Japan

Key words neuron · mesenchymal stem cell · Noggin · methylation · transdifferentiation · bone morphogenetic protein · dedifferentiation

Introduction

Bone marrow stromal (BMS) cells were originally reported to constitute a microenvironment of bone marrow and to be a prerequisite for the proliferation of hematopoietic stem cells (Dexter et al., 1977). Various hematopoietic lineages can be grown on BMS cells under appropriate conditions. BMS cells communicate with hematopoietic cells and BMS cells through cell-to-cell signals from cytokines (Metcalf, 1985; Umezawa et al., 1991), membrane-bound molecules, the extracellular matrix (Roberts et al., 1998), and gap junctions (Umezawa et al., 1990).

BMS cells *per se* are reported to have many characteristics of mesenchymal stem cells, which generate a progeny that can differentiate into multiple cell lineages (Fuchs and Segre, 2000). Pluripotent stem cells derived from marrow stroma may differentiate into various types of cell types, including bone (Rickard et al., 1994), muscle (Ferrari et al., 1998), fat (Harigaya et al., 1981; Umezawa et al.,1991), tendon, and cartilage (Ashton et al., 1980). Recently we have shown that marrow stroma is also a potential source of cardiomyocytes (Makino et al., 1999). Recent reports have shown that adult stem cells have a greater plasticity than previously thought (Bjornson et al., 1999; Petersen et al., 1999; Clarke et al., 2000), with BMS cells showing the potential to adopt totally different endpoints compared with their well-characterized mesenchymal derivatives (Pittenger et al., 1999), possibly including neural cells.

Cells from bone marrow exhibit neural phenotypes and marker expression when the cells migrate into the brain (Brazelton et al., 2000; Mezey et al., 2000). How-